SNE
SIMULATION NOTES EUROPE

ARGESIM

11th EUROSIM Congress, July 3-5, 2023, Amsterdam — EUROSIM 2023

The EUROSIM Congress 2023, the **11th EUROSIM Congress**, will be organized by DBSS, the Dutch Benelux Simulation Society, in Amsterdam, July 3-5, 2023.

This time, the EUROSIM Congress's theme is *Simulation for a sustainable future*. And there is no better place than Amsterdam to celebrate the link between simulation and sustainability. You will be pleased to discover the fascinating and vibrant city of Amsterdam, a hub for many sectors such as logistics, ICT, art, financial and business services, and fashion, among others.

<div align="center">

www.eurosim2022.eu

</div>

SIMULATION in Produktion und Logistik
13. – 15. SEPTEMBER 2023 | TECHNISCHE UNIVERSITÄT ILMENAU | GERMANY

Als größte europäische Simulationstagung für Produktion und Logistik präsentiert die ASIM Fachtagung alle zwei Jahre zukunftsweisende Trends und aktuelle Entwicklungen, wissenschaftliche Arbeiten sowie interessante Anwendungen in der Industrie. Der thematische Fokus der nächsten Fachtagung lautet Nachhaltigkeit in Produktion und Logistik. Damit greift die Tagung eine wichtige gesellschaftliche Thematik auf und fokussiert gleichzeitig auf aktuelle Forschungsthemen der Simulationswelt.

<div align="center">

www.asim-fachtagung-spl.de/

</div>

I3M 2023 — International Multidisciplinary Modeling & Simulation Multiconference — 18-20 September 2023, Athens, Greece — www.msc-les.org/i3m2023

Every year, the I3M Multiconference renovates the opportunity to bring together researchers, scientists and practitioners, from the Mediterranean Area, Latin & North Americas, Europe, Asia, Africa and Australia, who are concerned with Modeling and Simulation in Industry and Academia. As a result of the joint effort of many scientific excellences, I3M is an opportunity to meet and discuss and, as usually happens, constructive debate makes people open up, brings food for thoughts as well as new ways to explore encouraging multi-disciplinary cooperation and collaborations.

Winter Simulation Conference 2023 — Simulation for Resilient Systems — December 10-13, 2023, San Antonio, TX — www.wintersim.org

The Winter Simulation Conference 2023 highlights the vital role that simulation plays in designing, planning, and operating resilient systems under uncertainty. In an increasingly inter-connected world, it is more critical than ever to ensure that systems quickly recover from and adapt to major disruptions. With its uncertainty modeling and explainable analytics capabilities, simulation is one of the key technologies that lie at the heart of building resilient systems. We invite papers that emphasize the latest advances in simulation theory and applications showcasing the integrated use of simulation with technologies ranging from the Internet of Things and statistics to AI/ML and optimization. We particularly encourage applications of simulation to improve resiliency in a wide range of domains, including but not limited to aviation, disaster response, education, energy, finance, healthcare, infrastructure, manufacturing, national security, space systems, and supply chains.

Editorial

Dear Readers, This second issue of SNE Volume 33, 2023, underlines the astonishing broad area of modelling and simulation. Y. Shih's contribution 'Simulation of a Computational Model for the Performance Analysis of Mobile Police Bases in Apprehending Drug Dealers in the City of Itanhaém (São Paulo/Brazil)' and the contribution 'Raising Awareness of Climate Change Impact and Mitigation – The MyWorld Simulation Game' by U. Beyer, M. Karnassnigg, and O. Ullrich deal with exciting applications: crime prevention and awareness of climate change impacts. Three other contrasting contributions present applications in biology, train scheduling, and software service architecture: 'Modelling Blood Volume Oscillations in the Finger' by H. Kastinger and M. Bachler investigates a new technology for blood pressure measurement, 'Analysis of Train Delays using Bayesian Networks' by V. Barzal et al. tries to find free slots for freight trains in dense train public transport systems, and 'Service-Oriented Architecture for Automatic Evaluation of Urban Logistical Concepts' by V. Ahlers et al. presents a framework for combining general traffic models with specialized logistical models into singular simulations. And we are glad, that D. Jammer, P. Junglas, and S. Pawletta have finalized a benchmark study for ARGESIM's Parallel Benchmark CP2. The contribution 'Solving ARGESIM Benchmark CP2 'Parallel and Distributed Simulation' with Open MPI and Matlab PCT – Lattice Boltzmann Simulation' continues and completes the benchmark contribution from SNE 32(4), which presented the Monte Carlo and PDE case studies with the same technique.

The cover of this issue presents the second digital marbling graphics by Graham Horton, Professor for Simulation and Modelling at University Magdeburg, and ASIM-Member for many years, introduced in SNE 33(1). The title 'Italian Sisters' reflects a special technique for making marbled paper: two combs make the pattern.

I would like to thank all authors for their contributions for this issue, also and many thanks to the SNE Editorial Office for layout, typesetting, preparations for printing, electronic publishing, and much more. And we are glad that after the series of virtual conferences we can promote again EUROSIM face-to-face conferences: the EUROSIM Congress 2023, July 2023 Amsterdam, the conference ASIM SPL 2023, Ilmenau, in September 2023, I3M September 2023 in Athens, and others (see covers).

Felix Breitenecker, SNE Editor-in-Chief, eic@sne-journal.org; felix.breitenecker@tuwien.ac.at

Contents SNE 33(2)

e-SNE 33(2), DOI 10.11128/sne.33.2.1064

www.sne-journal.org/sne-volumes/volume-33

Basic e-Version with Open Access
Full e-Version for Members of publication-active EUROSIM
 Societies: ASIM, CSSS, DBSS, KA-SIM, NSSM, SIMS, SLOSIM, UKSIM
print-SNE for members on demand (printer INTU TU Wien)

Cover: Digital Marbling by Graham Horton, type 'Italian Sisters'; *digital-marbling.de*

SNE Contact & Info

SNE SIMULATION NOTES EUROPE

SNE - Aims and Scope

Simulation Notes Europe (SNE) provides an international, high-quality forum for presentation of new ideas and approaches in simulation - from modelling to experiment analysis, from implementation to verification, from validation to identification, from numerics to visualisation (www.sne-journal.org).

SNE seeks to serve scientists, researchers, developers and users of the simulation process across a variety of theoretical and applied fields in pursuit of novel ideas in simulation. SNE follows the recent developments and trends of modelling and simulation in new and/or joining areas, as complex systems and big data. SNE puts special emphasis on the overall view in simulation, and on comparative investigations, as benchmarks and comparisons in methodology and application. For this purpose, SNE documents the ARGESIM Benchmarks on *Modelling Approaches and Simulation Implementations* with publication of definitions, solutions and discussions. SNE welcomes also contributions in education in/for/with simulation.

SNE is the scientific membership journal of EUROSIM, the *Federation of European Simulation Societies and Simulation Groups* (www.eurosim.info), also providing Postconference publication for events of the member societies. SNE, primarily an electronic journal e-SNE (ISSN 2306-0271), follows an open access strategy, with free download in basic version (B/W, low resolution graphics). Members of most EUROSIM societies are entitled to download e-SNE in an elaborate full version (colour, high resolution graphics), and to access additional sources of benchmark publications, model sources, etc. (via group login of the society), print-SNE (ISSN 2305-9974) is available for specific groups of EUROSIM societies.

SNE is published by ARGESIM (www.argesim.org) on mandate of EUROSIM and ASIM (www.asim-gi.org), the German simulation society. SNE is DOI indexed with prefix 10.11128.

Author's Info. Individual submissions of scientific papers are welcome, as well as post-conference publications of contributions from conferences of EUROSIM societies. SNE welcomes special issues, either dedicated to special areas and/or new developments, or on occasion of events as conferences and workshops with special emphasis.

Authors are invited to submit contributions which have not been published and have not being considered for publication elsewhere to the SNE Editorial Office.

SNE distinguishes different types of contributions (*Notes*), i.e.

- **TN** Technical Note, 6–10 p.
- **SN** Short Note, max. 5 p.
- **SW** Software Note , 4–6 p.
- **BN** Benchmark Note, 2–10 p.
- **ON** Overview Note – only upon invitation, up to 14 p.
- **EN** Education Note, 6–8 p.
- **PN** Project Note 6–8 p.
- **STN** Student Note, 4-6 p., on supervisor's recommendation
- **EBN** Educational Benchmark Note, 4–10 p.

Further info and templates (doc, tex) at SNE's website, or from the Editor-in-Chief

www.sne-journal.org

office@sne-journal.org, eic@sne-journal.org

Simulation of a Computational Model for the Performance Analysis of Mobile Police Bases in Apprehending Drug Dealers in the City of Itanhaém (São Paulo/Brazil)

Yung-Chin Shih[1*]

[1]Department of Production Engineering, Federal University of Technology of Paraná, R. Doutor Washington Subtil Chueire, 330, 84017-220, Ponta Grossa, Paraná, Brazil; *chin@utfpr.edu.br

Abstract. In this study, we developed a computational model to simulate the number of arrests made by police when using mobile police bases. For a simulation period of twelve months, the results showed that the use of more mobile bases did not always lead to more arrests. Moreover, it was observed that if an equal distribution of police officers might jeopardize the number of arrests. We proposed an unbalancing model in order to promote the police workload distribution. The simulation showed that the model can produce beneficial results with only a negligible imbalance.

Introduction

According to [3], Brazil is plagued by extreme violence, originating from multiple factors such as its poor economic condition, cultural differences, and wars between factions. For every 100,000 inhabitants, Brazil sees 27.1 homicides. Much of this violence can be attributed to organized crime linked to drug trafficking [11]. Therefore, curbing any form of trafficking, regardless of its nature, can help reduce the number of homicides.

As mentioned by [12], the implementation of the pacifying police unit (UPP) is strategic and is based on geoprocessing; it identifies regions with a high incidence of theft. However, as the world of crime is highly dynamic, many of the UPPs in Brazil have been replaced by mobile modules.

A mobile module (or mobile police base) is a vehicle that reinforces ostensive patrolling, bringing the police closer to the community, in addition to favoring the arrival of police officers when there is a crime-related incident.

According to [7], by patrolling through mobile police bases, the police can typically respond to drug-related incidences within a 2 km radius, while some authors argue that they can cover a greater distance. The module can remain at a certain location and even change its position in response to a specific incident.

In each mobile police base, a team patrols its surroundings and makes arrests if it identifies a crime. Police officers can perform patrolling in several ways, including in motorcycles, bicycles and even on foot. According to [2], the use of mobile police bases aims to reduce crime with low offensive potential.

According to [6], the city of Itanhaém (located on the coast in the state of São Paulo, Brazil) has the highest rate of exposure to violent crime. Hence, attempts to reduce such crime are prioritized by municipal authorities.

With this background, in this study, we developed a computational model to predict the performance of mobile police bases in apprehending illicit drug traffickers. The model runs using information for the city in question.

The remainder of this paper is divided into four sections. The first part describes the methods used in the research, methodology, and types of data collected. The model used in the simulation is discussed in the second part. The third part presents the results (obtained under balancing/unbalancing conditions), discussion of the results, and statistical analysis. Finally, we draw our conclusions.

1 Material and Methods

The method chosen for this study was a computational model, and the computational results obtained were quantitative, that is, the number of arrests, the size of the vulnerable area not covered by police bases, and the total cost incurred by the city hall. Because of the difference between the distribution of traffickers along the crowns as shown in fourth section, the performance of the arrests carried out by the police may be jeopardized, mainly due to the lack of police. Thus, an unbalanced model based on the workload was proposed. The results were compared with those obtained using a balanced model.

2 Model Police / Drug Dealer

2.1 Determining the coverage and vulnerable areas

Let $N_{current\ period}$ mobile police bases be randomly located in the total area of the city, denoted by A_T. The coordinates can be represented as $(x_{i=1}, y_{i=1}) \neq (x_{i=2}, y_{i=2}) \dots \neq (x_{i=\text{N current period}}, y_{i=\text{N current period}})$.

If the coverage radius of each mobile police base i is R_i, the areas supervised by all the police bases are (1):

$$OA_{Ncurrent\ period} = \sum_{i=1}^{Ncurrent\ period} \pi . R_i^2 \qquad (1)$$

As R_i can assume any positive value, an overlapping area may exist. If there are K overlapping areas with L police stations, the area occupied by police bases can be expressed as (2):

$$OA'_{Ncurrent\ period} = \\ OA_{Ncurrent\ period} - \sum_{L=2}^{N} \sum_{ii=1}^{K} OLA_{L,ii}, \\ \text{with } L \, \forall \, i \qquad (2)$$

Here, OLA represents the overlapping area, and ii is the counter of K overlapping areas. For example, if $L = 3$ and $K = 4$, there are four occurrences in the three overlapping areas.

Thus, the remaining (vulnerable) areas represented by the RA variable can be expressed as follows (3):

$$\begin{cases} RA_1 = A_T - OA_{Ncurrent\ period} \; \ll== \\ \quad without\ overlapping\ area \\ RA_2 = A_T - OA'_{Ncurrent\ period} \; \ll== \\ \quad with\ overlapping\ area \end{cases} \qquad (3)$$

If RA (both) is the region farthest from police stations, i.e., the preferred area for criminals, then the objective is to minimize RA.

The focus here is on dealing with nonoverlapping areas covered by the police bases; then, we can represent RA_1 through expressions (4), (5), and (6):

$$min\ RA_1 = A_T - \max\{OA_{Ncurrent\ period}\}, \\ \text{where } 0 < \max\{OA_{Ncurrent\ period}\} < A_T \\ \text{to avoid } RA_1 \text{ becoming negative} \qquad (4)$$

$$min\ RA_1 = A_T - \pi \cdot max\{ \sum_{i=1}^{Ncurrent\ period} R_i^2 \}, \\ \text{with } \pi \cdot max\{\sum_{i=1}^{Ncurrent\ period} R_i^2\} \le A_T \qquad (5)$$

$$min\ RA_1 = A_T - \pi \cdot \{\max R_1^2 + \max R_2^2 + \\ + \cdots + max\ R_{Ncurrent\ period}^2 \} \qquad (6)$$

From these expressions, it can be noted that while the coverage radius are different, it is not possible to maximize each R_i. To achieve the highest value of R_i, it is necessary for all of them to be equal by positioning them as equidistantly as possible between the police bases. Thus, the expression can be summarized as (7):

$$\{ min\ RA_1 \} = A_T - N_{current\ period} \cdot \pi \cdot R^2 \qquad (7)$$

2.2 Equidistant positioning of police bases

To calculate RA_1, two unknown variables must be defined that are mutually dependent. In the case of equidistant positioning of police bases, the variables are inversely proportional ($N_{current\ period}$ and R).

Once $N_{current\ period}$ is defined, it is possible to determine R and the desired value of RA_1.

For a given value of $N_{current\ period}$, with the expression proposed by [1], called the distribution degree Φ shown in (8), the shortest distance between equal objects can be as large as possible. The unit of measurement was distance.

The authors used this expression to define the positions of machines in a physical arrangement study on factories. The lower the degree of distribution, the better the result; that is, the more equidistant the objects. Similarly, police bases (equal objects) can be positioned equidistantly.

To obtain one of the variables described in (8), we need to solve (9):

$$\Phi = \sum_{j=1}^{NO} \sum_{n_j=1}^{NO_j} \frac{\delta_{n_j}}{NO \cdot NO_j} \qquad (8)$$

$$\delta_{n_j} = \sum_{k \neq j}^{N} d^*_{n_j k} \qquad (9)$$

Here $d^*_{n_j k}$ is the distance between the n^{-th} object of type j and the closest object of type k; $n_j = n^{-th}$ object type j; NO_j is the number of objects type j; NO represents the types of objects.

In this study, NO is equivalent to $N_{current\ period}$. To computationally obtain the distribution degree, the authors argue that metaheuristics should be used to obtain the degree of distribution. This is because the computer tests different positions that each police base can occupy, thus reducing the computational search time. The distribution degree is calculated for each police base allocation.

[8] developed a genetic algorithm (GA) to determine the distribution degree. When performing numerous trials (generations in the GA), the degree of distribution that presents the lowest degree of distribution is the most equidistant possible placement between objects. Therefore, in this study, we developed a GA. Because there are only two types of objects (police bases and positions not occupied by police bases), it is not necessary to perform many generations in this case.

Finally, it is possible to calculate the distance between police bases and consequently obtain the desired circular radius (10):

$$
\begin{aligned}
R = \frac{1}{2} \cdot \min\{ & SQRT[(x_{i=1} - x_{i=2})^2 + (y_{i=1} - y_{i=2})^2]; \\
& SQRT[(x_{i=1} - x_{i=3})^2 + (y_{i=1} - y_{i=3})^2]; \dots; \\
& SQRT[(x_{i=Ncurrent\ period-1} - x_{i=Ncurrent\ period})^2 + \\
& + (y_{i=Ncurrent\ period-1} - y_{i=Ncurrent\ period})^2]\}
\end{aligned} \quad (10)
$$

2.3 Determining the number of police officers and the number of drug dealers

The total number of police officers working in a region is considered. Using $Y\%$ (the percentage of police officers working in regions covered by police bases), we can calculate the number of police officers per police base ($n_{i\ police}$). Therefore, the difference $(1 - Y)\%$ corresponds to the effective personnel working in vulnerable regions, under the condition that $Y\% > (1 - Y)\%$.

For the total number of traffickers operating in the region, if $X\%$ operate in vulnerable areas, the remaining $(1 - X)\%$ will operate in coverage areas.

These established inequalities are due to the fact that police officers are at a greater risk in more vulnerable areas. However, it is not convenient for traffickers to operate close to police bases because these areas are a greater risk to drug dealers.

For a given number of mobile bases N, it is possible to estimate the number of traffickers for each mobile base i, represented by $n_{i\ drug\ dealers}$.

The coverage area of each police base i was divided according to the number of circular crowns adopted. For example, if there are two crowns, the height of each crown is $R/3$. In addition to the two circular crowns, there will be an internal circle with a radius of $R/3$. It can simply be called a circular crown. In these cases, the area of the circular crown will always be greater than that of the adjacent interior.

The number of police officers at each police base was equally distributed by each circular crown. For traffickers, the preferred active areas are external crowns.

The initial positions of each police officer and each drug dealer are different from each other and randomly established. For each police base, we established an arrest performance target to be used in decisions regarding hiring police officers. The target is defined as the expected number of arrests EA_i.

2.4 Determining the number of arrests and calculating the total cost

As the simulation progressed, new values of N were obtained, which in turn changed the configuration of police base positions in the A_T area. This is because, if the number of arrests reaches a certain number, physical structures with a mobile police base will be required.

The number of arrests carried out on a given day depends on the movement of traffickers and police. However, their movements differed. In the case of the drug dealer, the subject performed move–stop exercises.

Considering the time for which the dealer remained in the same location, this can be represented by the following equation (11):

$$
\frac{S_1}{v_1} + \frac{S_2}{v_2} + \cdots + \frac{S_n}{v_n} = WJDD - n \cdot t_{standing\ up} \quad (11)
$$

where $WJDD$ represents the work journey of the drug dealer; n represents the number of dealers; s represents the distance traveled by each trafficker; v represents the displacement speed of each trafficker; and t represents the time spent at the site.

If the speed is constant throughout the path taken and represents all the distances by $\bar{S}$, then the expected number of locations reached on the workday is (12):

$$
\begin{aligned}
N_{locations\ drug\ dealer} = \\
WJDD / \left(\frac{\bar{S}_{drug\ dealer}}{v_{drug\ dealer}} + t_{standing\ up} \right) \quad (12)
\end{aligned}
$$

In the case of a police officer, movement is interrupted only to apprehend a drug dealer. Hence, we omitted the stop time. The expression is shown in (13):

$$\frac{S_1}{v_1} + \frac{S_2}{v_2} + \cdots + \frac{S_{n'}}{v_{n'}} = WJPO \qquad (13)$$

where $WJPO$ is the work journey of the police officer; n' represents the number of police officers; s represents the distance traveled by each officer; v represents the displacement speed of each officer.

If we assume that the displacement speed of the police officer is constant and if we represent all distances covered by $\bar{S}$, then the expected number of locations that can be reached by the police officer can be expressed by (14):

$$N_{locations\ police\ officer} = WJPO / \left(\frac{\bar{S}_{police\ officer}}{v_{police\ officer}} \right) \quad (14)$$

When both the locations are identical, an arrest occurred. Due to the arrests, the number of drug dealers is subtracted. The police officer sends a delinquent to a mobile base for registration and other administrative activities. Therefore, the on-site actions of the officer become inactive. Activity is resumed only the following day. The subtracted number of traffickers is immediately replenished the following day.

Therefore, the ratio of the number of police officers to the number of drug dealers can be expressed as (15):

$$f = \frac{N_{locations\ police\ officer}}{N_{locations\ drug\ dealer}} \qquad (15)$$

For example, if the result of f is eight, this indicates that there are eight police movements reaching eight different locations against one trafficker movement (reaching one new location). The variable f corresponds to the number of loops to be executed by the computational model to determine new police positions based on the number of positions reached by the traffickers. Thus, for each i, if the positions of the dealer and police are the same, then an arrest is made ($A_{i\ current\ period}$).

For the entire month, the total cost can be calculated as follows (16):

$$TC = PC \cdot \sum_{i=1}^{N} n_{i\ police} + N \cdot SPC \qquad (16)$$

where TC represents the total cost; N represents the number of mobile bases; n represents the number of police officers in base i; PC represents the cost incurred in the deployment of each police officer; and SPC represents the monthly cost to maintain the physical structure of each mobile base.

The sum of officers from all mobile police bases must be calculated because this information is used to determine the number of officers from each mobile base in the next period. The total number of police officers operating in the coverage areas is (17):

Total number of police officers $_{current\ period}$ =

$$= \sum_{i=1}^{N\ current\ period} n_{i\ current\ period} \qquad (17)$$

2.5 Updating the number of police officers and drug dealers for the next period

The updated number of police officers for the following month is based on the expected number of arrests.

The number of police officers required for each mobile base i in the next period can be calculated using Equations (18), (19), and (20). If the number of arrests in the current period is higher than the expected number, the difference must be added to the current number of police officers (18). If the number of arrests in the current period is lower, the difference must be subtracted (19). However, the number of police officers remains the same (20):

- If $A_{i\ current\ period} > EA_i$ then $n_{i\ next\ period} =$
$$= n_{i\ current\ period} + [A_{i\ current\ period} - EA_i] \quad (18)$$

- If $A_{i\ current\ period} < EA_i$ then $n_{i\ next\ period} =$
$$= n_{i\ current\ period} - [EA_i - A_{i\ current\ period}] \quad (19)$$

- If $A_{i\ current\ period} = EA_i$ then
$$n_{i\ next\ period} = n_{i\ current\ period} \qquad (20)$$

We established the total number of police officers required for the next period (21) as follows:

Total number of police officers $_{next\ period}$ =

$$= \sum_{i=1}^{N\ current\ period} n_{i\ next\ period} \qquad (21)$$

The difference d, expressed in Equation (22), between the number of police officers in the current period and that in the next period determines whether there is a need to change the number of mobile bases. When the cost of the required police officers is greater than the cost of the mobile base, more mobile bases are added:

d = Total number of police officers $_{next\ period}$ -
Total number of police officers $_{current\ period}$ (22)

Thus, we can establish some rules, as expressed in equations (23) and (24).

If the difference is positive,

$$d \cdot PC \geq SPC + n_{i\ current\ period} \cdot PC \\ N_{next\ period} = N_{current\ period} + 1 \quad (23)$$

If the difference is lower than or equal to zero, then

$$|d| \cdot PC \geq SPC + n_{i\ current\ period} \cdot PC \\ N_{next\ period} = N_{current\ period} - 1 \quad (24)$$

With the new value of $N_{next\ period}$ determined, we can obtain R and consequently the values of RA_1 and so on.

Regarding the number of traffickers, the integration of new traffickers occurs daily. This implies that the total number of traffickers is always fixed.

3 Simulation of the Model

3.1 Definition of the input parameters and discussion of results

The city of Itanhaém (in São Paulo) has an estimated area of 600 km^2 according to [9]. [4] recorded that the average estimate in the state of São Paulo is one police officer per 488 inhabitants. Thus, according to [9], if the city of Itanhaém has approximately 103,000 inhabitants, the city is estimated to have 211 police officers. There is no precise information on the number of drug dealers in the cities in São Paulo. However, if we use [5]'s data as a reference, which states that the ratio is four drug dealers per police officer in Rio de Janeiro, we estimate approximately 800 drug dealers.

The available software for building such a computational model is Dev-Pascal (Pascal language); the simulation was done on a PC with i3-10100 CPU, 8 cores, 3.6 GHz, 4.1 GB of RAM.

Based on the information obtained from the aforementioned city, in this study, the dimensions were set to 25 km × 25 km; the total number of available police officers in the city was 250 and updated monthly. The total number of traffickers operating throughout the city was fixed at 1000. The initial number of mobile police bases was 13 ($N_{initial} = 13$), and $Y\%$ was taken as 70%. Therefore, the number of police officers working in mobile bases was 250; $Y\% = 175$, and in vulnerable areas, there were 75 police officers.

The number of traffickers with $X\% = 80\%$ that are active in vulnerable areas was 1000; in coverage areas, $X\% = 800$, and the number of traffickers was 200. Thus, per police base, the estimate was

$$n_{i\ police\ officer} = trunc\ (175 / N_{i\ initial}).$$

The number of traffickers acting per police base could be estimated through

$$n_{i\ drug\ dealers} = trunc\ (200 / N_{i\ initial})$$

The dealer distributions for the three circular crowns (interior to exterior) were 0%, 20%, and 80%. The trafficker's working day was established using the relationship

$$WJDD = 3h; \quad v_{drug\ dealer} = 0.7\ \text{m/s};$$
$$\bar{S}_{drug\ dealer} = 10\ \text{m}; \quad t_{standing\ up} = 0.25\ \text{h};$$
$$v_{police\ officer} = 35\ \text{km/h}; \quad \bar{S}_{police\ officer} = 40\ \text{m}.$$

PC corresponds to the salary and fuel cost per month = R\$5000.00; SPC corresponds to fuel and van rental per month = R\$20.000,00; $EA_i = 40\%$ de $n_{i\ police}$.

To run the GA, we adopted five generations with 20 individuals in the population, a probability of 80% for crossover, and 2% for mutation.

Table 1 presents the simulation results. The first row shows the performance when 13 mobile police bases were used, resulting in 359 arrests. The outermost circular crowns saw a greater number of arrests. The vulnerable area not covered by police bases was 461.64 km^2, with a total cost of R\$1105K.

The results showed that the installation of more police bases cannot always increase the number of arrests, as was the case between months 4 and 8.

By separately analyzing the results of the two groups, we found that the number of arrests in the case of more mobile bases (from 10 to 13) averaged at 723.25, and the number of arrests in the case of fewer bases (7 to 9) averaged at 768.5. From this, we can conclude that, in general, a greater number of mobile bases does not necessarily result in a greater number of arrests.

The results showed that working with more police bases does not always result in a lower vulnerable area.

By observing the three-performance metrics, namely the "total arrests," "vulnerable area," and "total cost," it is not possible to reach the best value considering all the three metrics. Notably, the reduction in the number of police bases seems to have a strong influence on the total cost reduction, as was the case in months six to seven as well as in months three to four.

Statistically, if the number of traffickers at the beginning of each month is defined as 1000, and if we consider that 80% of months should have more than 1000 arrests, it indicates that the number of circular crowns used produces a satisfactory performance.

Month	Number of mobile police bases	Number of arrests			Total arrests	Vulnerable area (km²)	Total cost (R$)
		First crown (innermost)	Second crown	Third crown (outermost)			
1	13	0	154	205	359	**461.64***	1105K
2	12	0	444	713	**1157***	587.30	1080K
3	11	0	452	571	**1023***	590.44	1045K
4	10	0	103	251	354	**467.92***	1050K
5	9	0	276	507	783	561.38	1035K
6	8	0	273	433	706	562.17	**1000K***
7	7	0	332	531	863	570.02	**980K***
8	7	0	379	636	1015	581.02	**980K***
9	7	0	354	539	893	570.02	**980K***
10	7	0	324	544	868	570.02	**980K***
11	7	0	223	377	600	531.54	**980K***
12	7	0	152	268	420	487.56	**980K***
Total					9041		

Table 1: Simulation results, with three circular crowns, registered at the end of each month, throughout the months of the year. Two best values are highlighted.

Statistically, if the number of traffickers at the beginning of each month is defined as 1000, and if we consider that 80% of months should have more than 1000 arrests, it indicates that the number of circular crowns used produces a satisfactory performance.

We observed that three of the 12 months saw arrests above 1000. Therefore, the value of p was 3/12 = 0.37. So we can formulate the following hypotheses for the statistic p:

- H_0: $p \geq 0.8$, if 80% of the months have a performance equal to or greater than 1000 arrests,   (25)
- H_1: $p < 0.8$ otherwise.

The value of Z_{test} used in the comparison is

$$Z_{test} = (\hat{p} - p) \ / \ \sqrt{\frac{p(1-p)}{n}} \qquad (26)$$

The Z_{test} value was −3.72. For a level of significance of 5%, because -3,72 is lower than $Z_{\alpha=5\%} = -1.64$, the decision was to reject H_0.

3.2 Adaptation of the simulation model with implementation of imbalance

Imbalance per area

Note that when dividing the circumference and equally distributing the number of police in n crowns, the number of arrests in the internal crown was zero, and drug dealers were not involved.

In this study, traffickers preferred external crowns farthest from the base. This led to the idea that police officers should be reallocated differently.

This paper presents two unbalanced procedures. First, police officers are proportionally allocated according to the crown area.

Let p' be the probability that a police officer is located in a given circular crown. If the area increases, then to maintain the same p', a larger number of police officers should be assigned (27).

The steps are as follows:

- Calculate the total coverage area of base i.
- Calculate the percentage of each circular crown p';
- Calculate the number of police officers per ring crown using the following equation:
  Police officers in the circular crown
  $$= n_{i \, police \, officer} \cdot p' \tag{27}$$

Table 2 shows the results of the imbalance model. Clearly, a different number of police officers should be allocated to each crown to ensure a greater number of arrests. Surprisingly, the performance in the case of four circular crowns approached that in the case of three circular crowns. Thus, the variation in the number of circular crowns with unbalancing does not seem to jeopardize the arrest performance.

	Total arrests	
Month	Balanced	Area-based imbalance
1	359	552
2	1157	508
3	1023	1007
4	354	1591
5	783	3187
6	706	936
7	863	981
8	1015	741
9	893	1834
10	868	348
11	600	841
12	420	378
Total	9041	12904

Table 2: Comparison between the results obtained under balancing and unbalancing conditions by areas.

We note that the unbalancing model outperforms the balancing model.

Applying the statistical test to the unbalanced results, we find that the p value was $4/12 = 0.33$. The value of Z_{test} was -4.07, resulting in the rejection of the hypothesis H_0.

We conclude that, although the number of arrests improved overall, it still did not satisfy the monthly performance conditions.

During the simulation, with the change in the number of mobile bases, the number of traffickers per police base also changed. This means that, for the current approach, the number of police officers remain unchanged, consequently reducing the number of arrests.

This suggests that a greater workload should be assigned to police officers in the most distant crowns. This is the method proposed in this study.

Imbalance per workload

The results suggests that a greater workload should be assigned to police officers in the most distant crowns. This is the method proposed in this study, Equation (28):

$$\beta = \frac{n_{i \, police \, officers} \cdot WJPO}{\Delta + (\sum_{i=0}^{\Delta-1} i) \cdot \alpha} \tag{28}$$

where β corresponds to the workload of the outermost crown; α corresponds to the imbalance factor; Δ corresponds to the number of circular crowns.

Once this value was determined, the other values were assigned according to the circular crown. The closer to the mobile police base, the lower the workload, indicating fewer police officers.

The workload CHS (29) of the εth crown counted from the base can be expressed as follows:

$$CHS = \beta + (\Delta - \varepsilon) \cdot \alpha \cdot \beta \tag{29}$$

Note that in Equation (28), α depends on the number of police officers operating in each police base (which varies temporally), β value, the number of circular crowns, and police's work journey. This means it is not possible to establish a fixed value of α.

To define the required range of α for the simulation, we use the input parameters under the condition that $\beta \geq 0$. If the police officer workday is 8 hours, then we can deduce that for $\beta \geq 8$, we must use $\alpha > -1$, in addition to $\alpha \neq 0$. Only negative values were used because of the higher workload in the external crown. Therefore, the α values for the three crowns were -0.9, -0.45, -0.15.

Table 3 shows the results. The benefits can be verified when a higher unbalancing factor (close to balanced $\alpha = 0$) is used.

As the value decreases (the greater the unbalancing), the benefits become evident, confirming that the unbalancing should be based on the workload.

Months of the year											
α=-0.15											
Crown 1	0	0	0	0	0	0	0	0	0	0	0	0
Crown 2	121	365	381	158	544	190	103	138	227	250	312	68
Crown 3	413	936	981	543	1298	516	376	402	582	696	857	230
Unbalanced	534	1301	1362	701	1842	706	479	540	809	946	1169	298
α=-0.45											
Crown 1	0	0	0	0	0	0	0	0	0	0	0	0
Crown 2	139	343	268	149	317	501	219	199	247	285	229	457
Crown 3	506	1274	1096	816	1238	1811	1108	995	1042	1087	1073	1656
Unbalanced	645	1617	1364	965	1555	2312	1327	1194	1289	1372	1302	2113
α=-0.9											
Crown 1	0	0	0	0	0	0	0	0	0	0	0	0
Crown 2	166	211	703	296	529	353	853	885	437	441	468	499
Crown 3	2259	3004	4620	3923	4211	3499	4311	4557	4188	4399	4584	4118
Unbalanced	2425	3215	5323	4219	4740	3852	5164	5442	4625	4840	5052	4617

Table 3: Results with unbalancing.

So results are:

- For $\alpha = -0.15$, p is 4/12,
- for $\alpha = -0.45$, p is 10/12 = 0.83,
- and for $\alpha = -0.9$, p is 12/12 = 1.

The corresponding Z_{test} values were calculated to be 4.07, 0.26, and 1.73, respectively.

Table 4 presents a comparison with the reference z at a significance level of 5%.

	-0.15	-0.45	-0.9
Unbalanced	-4.07 < -1.64	0.26 > -1.64	1.73 > -1.64
Decision	Reject H$_0$	Accept H$_0$	Accept H$_0$

Table 4: Statistical comparison with unbalancing.

4 Conclusions

In this study, a computational model was constructed for effective policing against drug trafficking, with the objective of simulating performance projections in cases where mobile police bases were implemented, aiming to increase the number of arrests, reduce the number of vulnerable areas, and reduce associated costs.

Using the computational model constructed for this purpose, it was possible to obtain the desired results for a performance comparison. The computational model proved to be versatile, as it could simulate possible changes in the positions of mobile bases, police officers, and particularly drug dealers.

The results showed that when there were areas with police supervision with a low circulation of traffickers, the expected result should be zero arrests, which was verified. This finding suggested that an unbalanced model can be used to reallocate officers in a different manner. When considering the imbalance by the area size (i.e., the larger the area, the higher the number of police officers, or vice versa), more arrests could be made.

Despite the benefits of unbalancing by area size, redistribution might fail. This is because, as the simulation progresses, the numbers of drug dealers and police officers might change. Hence, an unbalanced model was proposed according to the workload of the police officers. With the proposed model and using an intermediate lower value of the unbalancning factor, the obtained results were more promising.

As a proposal for future work, some restrictions could be considered, such as in areas that are difficult for police to access and are already dominated by armed traffickers. This prevents the installation of mobile bases in such locations. As a suggestion for future work, due to the limitations of the software used in this study, it was not possible to analyze the arrests made in areas not covered by police bases. As stated by [10], it is in the peripheries that crime is more organized, suggesting a way that aims to maintain a protection network and eliminate possible competitors. We also suggest the development of new unbalanced models in future studies.

References

[1] Benjaafar S, Sheikhzadeh M. Design of Flexible Plant Layouts, *IIE Transactions*. 2000; 32(4): 309-322. DOI 10.1023/A:1007691303186

[2] Costa AEF. *The violence prevention strategy through the community police in Alagoas: a management analysis, challenges and prospects* (in portuguese). Rio de Janeiro: ESG, 2019.

[3] Cruz JM. State and Criminal Violence in Latin America. *Crime, Law and Social Change*. 2016; 66: 375-396. DOI 10.1007/s10611-016-9631-9

[4] Exame. The States with the Highest Shortage of Police Officers per Inhabitant (in Portuguese), 2019. Available from: https://exame.com/brasil/brasil-tem-deficit-de-20-mil-policiais-em-seu-efetivo/.

[5] Feliciano J. Number of Traffickers in The State May be Four Times Greater Than That of Military Police. 2019. Available from: https://eurio.com.br/noticia/6544/numero-de-traficantes-no-estado-pode-ser-quatro-vezes-maior-que-o-de-policiais-militares.html.

[6] Santos GI. Four Cities in Baixada Santista Are Among the 10 Most Exposed to Violence in SP (in portuguese), 2020. Available from: https://g1.globo.com/sp/santos-regiao/noticia/2020/08/21/quatro-cidades-da-baixada-santista-estao-entre-as-10-mais-expostas-a-violencia-em-sp.ghtml.

[7] Garcia PM. PM's General Command Responds to Questions About Security in Curitiba (in Portuguese), 2022. Available from: https://www.curitiba.pr.leg.br/informacao/noticias/em-tribuna-livre-com-2-horas-de-duracao-pmpr-apresenta-balanco-das-atividades-de-2021.

[8] Gorgulho JH. Performance Analysis of Distributed Layouts in a Task Programming Environment with Manufacturing Sequence Flexibility (in Portuguese). Department of Mechanical Engineering, SP. University of São Paulo, 2006.

[9] IBGE. 2021. Available from: https://www.ibge.gov.br/cidades-e-estados/sp/itanhaem.html.

[10] Marques RG, Santos MA. The Crime of Drug Trafficking and the Relationship with Violence: an Interdisciplinary Contribution. *RP3 - Rev de Pesq em Pol Púb*. 2018; (1): 1-15.

[11] Miraglia P. Drugs and Drug Trafficking in Brazil: Trends and Policies, (date not informed). Available form: https://www.brookings.edu/wp-content/uploads/2016/07/miraglia-brazil-final.pdf.

[12] L. Sarzi, PM Changes Strategy and Adopts Mobile Modules in Curitiba. It Works? (in portuguese), 2019. Available from: https://www.tribunapr.com.br/caca-dores-de-noticias/curitiba/pm-muda-estrategia-adota-modulos-moveis-curitiba/.

Modelling Blood Volume Oscillations in the Finger

Hannah Kastinger[1*], Martin Bachler[1, 2]

[1]Institute for Analysis and Scientific Computing, TU Wien, Wiedner Hauptstraße 8-10,
   1040 Vienna, Austria; *martin.bachler@ait.ac.at
[2]Center for Health & Bioresources, AIT Austrian Institute of Technology, Giefinggasse 4,
   1210 Vienna, Austria; *hannah.kastinger@gmx.at

Abstract. The aim of this work is to describe a model of the relationship between blood volume and transmural pressure of a vessel of the finger, where the finger is pressed against a surface with increasing pressure. The focus lies on the amplitudes of the blood volume oscillations, as they can be measured easily. The model leads to a formula for the blood volume oscillation amplitudes. This equation is then fitted to measured data to estimate systolic and diastolic blood pressure. The focus lies on the fitting process and the quality of the fitting results.

Introduction

This work introduces and describes a model of the relation between blood volume and transmural pressure of a vessel of the finger which is pressed against a surface. More of interest than the absolute volume are in fact the blood volume oscillations, as they can be measured easily using an optical sensor, with respect to changes in the transmural pressure. This model for the blood volume oscillations shall be used for estimating the blood pressure without a cuff at the finger by fitting the model function to measured data and obtaining the systolic and diastolic blood pressure as fitting parameters.

1 The Model

The idea of the model is to describe a relation between blood pressure inside a vessel, pressure acting on the vessel from outside and the blood volume inside the vessel. The vessel of interest, the transverse palmar arch artery, is located in the finger tip and the situation of interest is the fingertip being pressed on some surface

with increasing pressure. This approach can be compared to the blood pressure measurement with a cuff around the upper arm as there is also an external pressure acting on the vessel. Similar to the finger pressing on a surface, the cuff is exerting decreasing pressure on the vessel from outside, while pressure oscillations are measured. First, let us take a look at the absolute volume of the vessel and afterwards at the blood volume oscillations in dependency of the external pressure acting on the vessel from outside.

1.1 The Vessel Volume

The transverse palmar arch artery lies parallel to the surface of the finger and the bone underneath. Let us assume the artery as a cylindric tube of length L. When the finger presses on a surface, the pressure also acts onto the wall of the vessel. This external pressure (P_{ext}) is directed inwards. [1]

The second relevant component is the blood pressure (P_b). This is the pressure applied on the vessel wall by blood running through the arteries. It is directed opposite to P_{ext}, in direction of the outer normal vector. Hence, the pressure acting on the vessel wall is a combination of P_b and P_{ext}. This combination is defined as transmural pressure P_t as follows:

$$||P_t|| := ||P_b|| - ||P_{ext}||.$$

A positive transmural pressure P_t means that the blood pressure P_b exceeds the external pressure P_{ext}. This leads to the vessel being pressed apart. A negative transmural pressure P_t, on the other hand, means that P_{ext} exceeds P_b and therefore the vessel is compressed. [1]

To find a relation between the transmural pressure P_t and the blood volume V of the artery, A is defined as the cross-sectional area of the artery. First we are looking at the artery in relaxed state: $P_t = 0$. In this case, we assume A as a circular disc with radius $R \in \mathbb{R}$.

In the second case we are looking at is $P_t < 0$. In this case, the artery is compressed. Figure 1 shows the cross-section with side length $a \in \mathbb{R}^+$ and radius of the semicircles $0 \leq r \leq R$. [1]
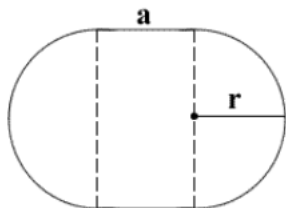

Figure 1: Schematic representation of the cross-section of the artery for a transmural pressure $P_t < 0$ [2].

The arterial wall is not stretched. We want to use this fact to find a relation between R, r and a. Let γ_0 be the boundary of A, the cross-section of the artery in relaxed state, then $L\gamma_0 = 2R\pi$. Let γ_s be the boundary of the deformed cross-section, then $L\gamma_s = 2r\pi + 2a$.

$$L\gamma_s = L\gamma_0 \tag{1}$$
$$2r\pi + 2a = 2R\pi \tag{2}$$
$$a = \pi(R - r) \tag{3}$$
$$\Rightarrow a \in [0, R\pi]. \tag{4}$$

If the artery is relaxed then $a = 0$ and if $a = R\pi$ the vessel is fully occluded. [1]

The next step is to find a relation between r and P_t. Let us define $r(t) := R(\sqrt{1 - e^{\alpha P_t}})$, $P_t < 0$, inspired by Charles. F. Babbs [3]. The parameter $\alpha > 0$ is related to the stiffness of the vessel wall. Now we can take a closer look at V.

$$V(P_t) = LA(P_t) = L(r(P_t)^2\pi + 2r(P_t)a) = \tag{5}$$
$$= LR^2\pi e^{\alpha P_t} = V_0 e^{\alpha P_t}, \tag{6}$$

where $V_0 := LR^2\pi$ is the volume of the relaxed vessel. We can see that a negative transmural pressure leads to an exponential reduction in blood volume. [1]

The next step is to look at the case $P_t > 0$. The wall is stretched uniformly in angular direction by the pressure. Hence, the cross-section A forms a circle with radius $r > R$. Let us define r in dependency of P_t based on Charles F. Babbs [3] as follows:

$$r(P_t) := R\sqrt{1 + \frac{\alpha}{\beta}(1 - e^{-\beta P_t})}. \tag{7}$$

The parameter $\beta > 0$ is also related to the stiffness of the arterial wall and is inversely proportional to the elasticity of the vessel wall. Again we want to take a look at the volume V:

$$V(P_t) = LA(P_t) = L(r(P_t)^2\pi =$$
$$= LR^2\pi(1 + \frac{\alpha}{\beta}(1 - e^{-\beta P_t})) =$$
$$= V_0(1 + \frac{\alpha}{\beta}(1 - e^{-\beta P_t})). \tag{8}$$

[1]

All together we can define the vessel volume V as follows:

Definition 1.1 (Vessel volume; P. Baumann [1], p. 42)
Let $L > 0$ be the length of the cylindric shaped transverse palmar arch artery and $R > 0$ the radius of the cross-section in a relaxed state ($P_t = 0$). Furthermore, let $\alpha, \beta > 0$ be fixed parameters describing the vessel wall elasticity and assume the deformation behaviour described previously. Then, V is given by

$$V : \mathbb{R} \to \mathbb{R}, P_t \longmapsto \begin{cases} V_0 e^{\alpha P_t}, & P_t < 0 \\ V_0(1 + \frac{\alpha}{\beta}(1 - e^{-\beta P_t})), & P_t \geq 0 \end{cases}. \tag{9}$$

With this definition we can see that $V \in C^1(\mathbb{R})$ and that it is monotonically increasing. Figure 2 shows the function of the vessel volume V for estimated values for α and β. [1, 3]
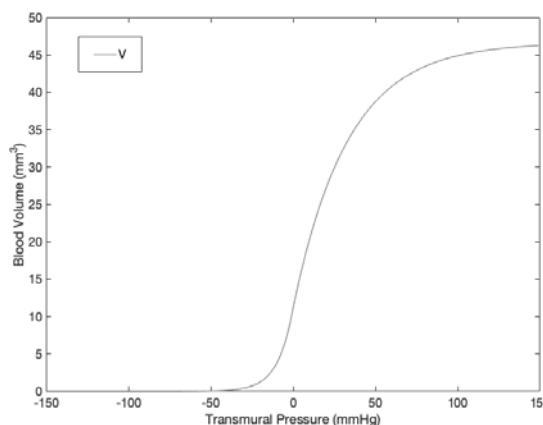

Figure 2: V for $\alpha = 0.11$ and $\beta = 0.03$.

1.2 The Oscillation Curve

The blood pressure P_b is not constant. In contrary, it varies between a minimum (diastolic, P_{dia}) and a maximum pressure (systolic, P_{sys}). If the external pressure increase at the finger is sufficiently slow, we can assume that P_{ext} is constant during each heartbeat. That means that the change of P_t is determined just by the variance of the blood pressure P_b. Furthermore, the differences of P_t lead to a varying amount of blood volume. Hence, V oscillates between its maximum and minimum during each cardiac cycle. Since V is monotonically increasing with P_t, it attains its minimum and maximum at the minimum and maximum of P_b. [1]

To make the next step let us first define pulse pressure $PP := P_{sys} - P_{dia}$. Now, we can define the maximum difference of blood volume ΔV during one heartbeat as follows:

$$\Delta V(P_m) := V(P_m + PP) - V(P_m). \quad (10)$$

P_m denotes the minimal transmural pressure which can also be calculated as $P_m = P_{dia} - P_{ext}$. [1]

The next step is to establish a connection between systolic and diastolic blood pressure and ΔV. First we will look at the case $P_m \leq -PP$:

$$\Delta V(P_m) = V_0 e^{\alpha(P_m + PP)} - V_0 e^{\alpha P_m} \quad (11)$$

The next case is $P_m \in (-PP, 0)$:

$$\Delta V(P_m) = V_0(1 + \frac{\alpha}{\beta}(1 - e^{-\beta(P_m + PP)})) - V_0 e^{\alpha P_m} \quad (12)$$

Last, we will take a look at the case $0 \leq P_m$:

$$\Delta V(P_m) = \quad (13)$$

$$= V_0(1 + \frac{\alpha}{\beta}(1 - e^{-\beta(P_m + PP)})) - V_0(1 + \frac{\alpha}{\beta}(1 - e^{-\beta P_m}))$$

[1]

As already mentioned above, $P_m = P_{dia} - P_{ext}$. Therefore

$$\begin{aligned} P_m + PP &= & P_{dia} - P_{ext} + P_{sys} - P_{dia} \\ &= & P_{sys} - P_{ext} \end{aligned}$$

Finally, we can combine these results and formulate an equation for ΔV:

$$\Delta V(P_{ext}) = \quad (14)$$

$$\begin{cases} V_0 \cdot e^{\alpha(P_{sys} - P_{ext})} - \alpha \cdot V_0 \cdot e^{\alpha(P_{dia} - P_{ext})}, \\ \qquad P_{ext} \geq P_{sys} \\ \\ V_0(1 + \frac{\alpha}{\beta}(1 - e^{-\beta(P_{sys} - P_{ext})})) - \alpha \cdot V_0 \cdot e^{\alpha \cdot (P_{dia} - P_{ext})}, \\ \qquad P_{dia} < P_{ext} < P_{sys} \\ \\ V_0(1 + \frac{\alpha}{\beta}(1 - e^{-\beta(P_{sys} - P_{ext})})) - V_0(1 + \frac{\alpha}{\beta} \cdot e^{-\beta(P_{dia} - P_{ext})}), \\ \qquad P_{ext} \leq P_{dia}. \end{cases}$$

[1]

Figure 3 shows the oscillation amplitude curve ΔV for an assumed systolic and diastolic pressure of 120mmHg and 80 mmHg and $\alpha = 0.11$, $\beta = 0.03$. [3, 4]
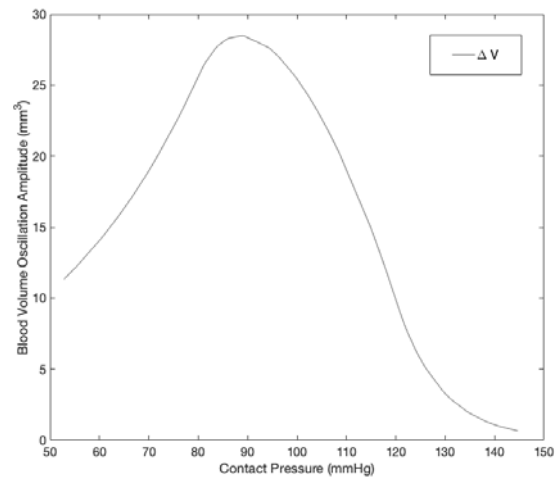
Figure 3: ΔV for $P_{sys} = 120mmHg$, $P_{dia} = 80mmHg$ and $\alpha = 0.11$, $\beta = 0.03$.

2 Estimating Blood Pressure via Model Fitting

This model, the formula for the blood volume oscillations ΔV in particular, in this form can be used for estimating blood pressure. To do so, equation 14 can be used as model function and be fitted to blood volume oscillations measured from the transverse palmar arch artery.

2.1 Measuring of the Blood Volume Oscillations

The blood volume oscillations (ΔV) are measured alongside the contact pressure (P_{ext}) by the smartPWA device. The smartPWA (smart Pulse Wave Analysis) device is a bio-signal acquisition sensor device specially developed and built by the AIT Austrian Institute of Technology (Vienna, Austria) for research projects. The device is intended to be held by the user with both hands, like a gamepad, as shown in Figure 4. The user's right index finger touches an optical sensor for photoplethysmography (PPG) to measure blood volume changes in the finger's microvascular bed. Below the PPG sensor is a pressure sensor that registers the contact pressure of the right index finger.

Figure 4: The smartPWA (smart Pulse Wave Analysis) and how it needs to be held: the right index finger touches an optical sensor for photoplethysmography to measure blood volume changes and the applied pressure with a pressure sensor below.

The PPG, and pressure signals are converted from analogue to digital signals at 256 Hz and 24-bit resolution. Communication with a smartphone or tablet computer is established via Bluetooth low energy (BLE) and the measured signals are streamed continuously to a mobile app for further data processing.

Let us take a closer look at the measurement of the blood volume oscillations. The finger pressure on the sensor is increased steadily by the user up to 200 mmHg over 30 seconds and at the same time the blood volume oscillations are measured with the PPG sensor. To obtain the best possible measurement, the contact pressure P_t between finger and sensor should increase linearly with respect to time t and the slope should not be steeper than 7 $\frac{mmHg}{s}$. Unfortunately, the pressure sensor currently in use is not able to detect pressure below 50

mmHg and therefore the pressure detection starts only at this value. Figure 5 shows an example for the contact pressure in orange. [1]
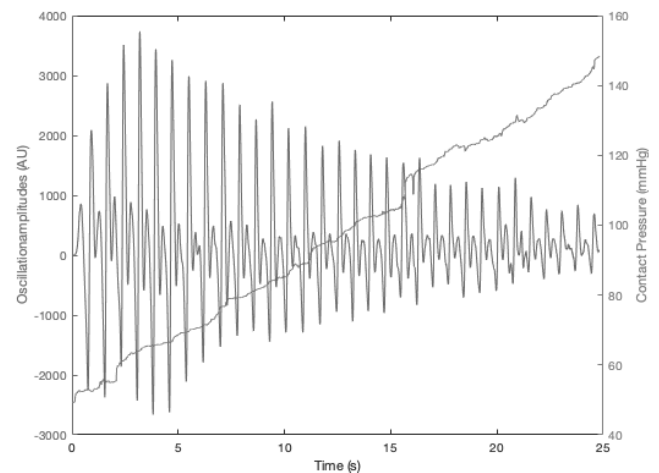

Figure 5: Example for a filtered measurement from the smartPWA. The oscillation amplitudes are shown in blue and the contact pressure is shown in orange.

To remove high frequency noise and slow signal drift, and enhance the amplitude of the volume oscillations, the measured signal from the photoplethysmography sensor needs to be filtered. We assume a heart rate of 60-120 beats per minute. Therefore, the filtering is done by applying a high-pass and a low-pass filter which combine to a band-pass filter with a frequency range of 1.9 Hz - 8.5 Hz. An example of this filtered signal is shown in blue in figure 5. [1]

2.2 Realization of the Model Fitting

The idea is to obtain the systolic and diastolic blood pressure as parameters of fitting the function ΔV to the measured data. This is done by classical model fitting. The fitting is realized in MATLAB (The MathWorks, Natick, Massachusetts, MA, USA) using the curve fitting toolbox. The fitting is done using the non-linear least squares method with a trust region algorithm as it is suitable if coefficient constraints are specified [5].

The measured data is prepared for the fitting process by selecting the peaks of the oscillations (marked in red in Figure 6). These peaks are used as the data points the model function shall be fitted to.

From input pressure P_{ext}, only those values are used for which there is also a peak present at the same time.
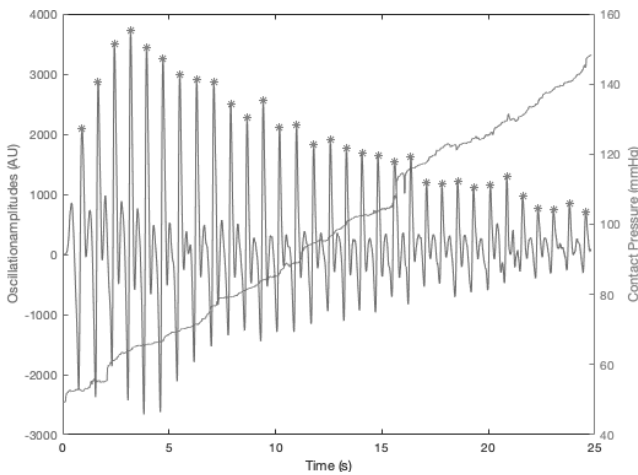
Figure 6: Oscillation amplitudes and corresponding contact pressure for an example measurement by the smartPWA. The peaks of the oscillations are marked in red.

The model function is, as previously mentioned, the function ΔV. Hence, there are five model parameters which need to be fitted: the two parameters α and β which are related to the stiffness of the arterial wall, the systolic and diastolic blood pressure which are the two values we want to obtain with this whole process, and the initial volume of the vessel V_0.

Initial Values and Limits. The MATLAB curve fitting tool box together with the Trust-Region algorithm allows us to set initial values, lower and upper limits for theses five parameters. To find useful values here, let us take a closer look at α and β first. We have already seen that $\alpha > 0$ and $\beta > 0$. Furthermore, it should always be true that

$$\frac{\beta}{\alpha + \beta} \approx \frac{1}{3}.[1] \qquad (15)$$

There is also an estimation of α and β for the brachial artery where the estimated values are

$$\alpha = 0.11 \text{ and} \qquad (16)$$
$$\beta = 0.03.$$

For these values the approximation (15) is far missed since $\frac{0.03}{0.11+0.03} \approx 0.21$. However, this can be explained by the fact that there are lots of different shapes of blood pressure curves. For some experiments, in this work the parameters α and β are also set to the values given in (16) and therefore the model function in these cases is $\Delta V(P_{sys}, P_{dia}, V_0; P(t))$. [3]

These facts need to be taken into consideration when choosing initial values and limits for α and β. As initial values, either the values given in equation (16) or $\frac{\text{upper limit - lower limit}}{2}$ for both are chosen. The lower limit is set 0.001 for both. Regarding the upper limits, there are several options, but especially equation (15) should be kept in mind. The used values are summarized in table 1. The values of each column are used in combination.

α	0.5	$\frac{2}{3}$	0.2
β	0.5	$\frac{1}{3}$	0.1

Table 1: Different options for the upper limits for α and β. The values of each column are used in combination.

Regarding the systolic and diastolic blood pressure, the initial values are chosen to be either $\frac{\text{upper limit - lower limit}}{2}$ for both or 120 for P_{sys} and 80 for P_{dia}, since these values are commonly known as reference values for blood pressure [4] . The upper and lower limit are set to the maximum and the minimum of the contact pressure P_{ext}, respectively.

Finally, for the initial volume V_0, we choose half of the difference between the maximum and minimum of oscillations of the blood volume as initial value and set the upper and lower limit to the said maximum and minimum.

The Data. From 26 subjects, 443 measurements have been taken at up to five points in time. If possible, for each subject and at each point in time, more than one measurement has been performed, to be able to compare repeated blood pressure estimations. Of the 26 subjects, 15 are male and 11 are female. From 6 of the 26 subjects, the age is unknown. The 1st quartile, median, and 3rd quartile of the birth-years of the other 20 subjects are 1982, 1985, and 1990. The earliest birth-year is 1972 and the latest is 1996.

2.3 Categorising of Measured Data

To optimize the results, one approach is to be more strict regarding the quality of the measurements. Two ways of deciding which measurement is good enough to be taken into account, are investigated. The first approach is to investigate the linearity of the contact pressure P_{ext} over time.
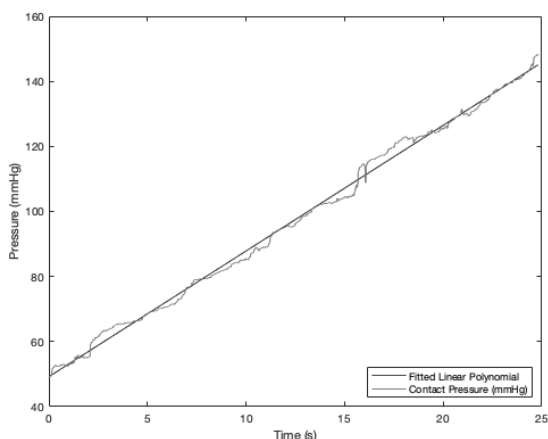
Figure 7: Plot of the contact pressure exerted on to the pressure sensor by the finger and the linear polynomial fitted to this curve.

Figure 8: Plot of the fitted curve and the used data points for an example measurement.

To do so, a linear polynomial is fitted to the contact pressure put to the sensor by the finger. This is done by the 'fit' function in MATLAB and the outcome can be seen in Figure 7. The quality of the measurement is then assessed with respect to the goodness of this linear fit. To find a threshold to decide which measurements to keep and which to reject, the sum of squares error (SSE_{lin}), R^2_{lin}, or root mean squared error ($RMSE_{lin}$) for a manually chosen subset of measurements are calculated, and the second quartile or median are used as guideline for the choice of a threshold.

Another approach to categorize the measurements is to accept or reject them with respect to the goodness of the model fitting (SSE_{mod}, R^2_{mod}, $RMSE_{mod}$). In this case, any criterion can be used and the threshold is chosen in the same way as above.

3 Results

The model fiting has been performed for all 443 measurements with different initial values and limits. Figure 8 shows the plot of the fitting curve and the data points for an example measurement using the above specified settings with initial values $\frac{\text{upper limit - lower limit}}{2}$ and upper limits 0.2 and 0.1 for α and β, respectively. The initial values for the systolic and diastolic blood pressure are also set to be $\frac{\text{upper limit - lower limit}}{2}$.

The fitted curve resembles the main properties of the model function ΔV (see figures 3 for reference). Furthermore, the fitted curve also fits to the data points

quite well.

However, there are not only positive results. Figure 9 shows an example where the model fitting did not work as expected.
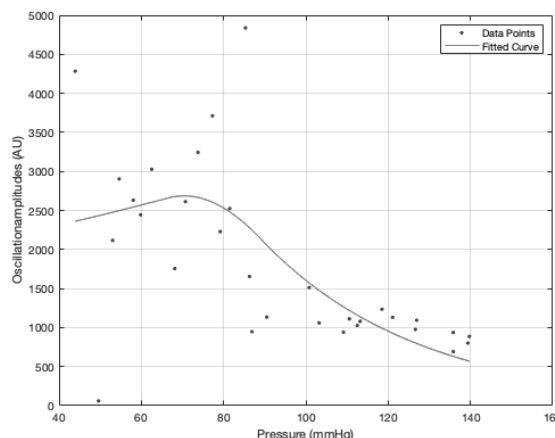
Figure 9: Plot of the fitted curve and the used data points for an example measurement.

To evaluate the quality of the fit more objectively, the goodness of the fit parameters provided by the MATLAB curve fitting toolbox are taken into consideration. For the above combinations of initial values and limits, these parameters are summarized in table 2. As can be seen clearly, there are almost no differences between the goodness of the fit parameters for all three combinations.

α	β	SSE	R^2	RMSE
0.5	0.5	1.0e+07* [0.1963 0.4722 1.1609]	0.4726 0.7502 0.8876	281.4590 432.8865 674.1670
$\frac{2}{3}$	$\frac{1}{3}$	1.0e+07* [0.1957 0.4710 1.1669]	0.4819 0.7522 0.8905	281.4213 432.3620 676.7246
0.2	0.1	1.0e+07* [0.1963 0.4793 1.1743]	0.4549 0.7483 0.8866	281.6088 432.8869 677.1325

Table 2: The 1st quartile, median and 3rd quartile of the goodness of the fit parameters for 443 measurements. SSE...sum of squares error, R^2...coefficient of determination, RMSE...root mean squared error.

3.1 Categorising of Measured Data

The categorization of the measurements to decide which are good enough for the estimation of the systolic blood pressure and which not is the next topic we want to look at. As discussed, two methods to do so are investigated in this work: fitting a linear polynomial to the contact pressure curve ('linear') and looking at the goodness of the fit of the model fitting ('model'). The threshold, i.e., the first quartile, median, and third quartile of the RMSE_{lin}, SSE_{lin}, and R^2_{lin} of the linear polynomial fitting calculated for a manually selected subset are given in table 3.

SSE_{lin}	R^2_{lin}	RMSE_{lin}
1.0e+04 * [3.2299 4.0901 5.9620]	0.9886 0.9922 0.9937	2.2565 2.5403 3.0695

Table 3: First quartile, median and third quartile of the dispersion of the goodness of the fit criteria SSE_{lin}, R^2_{lin}, and RMSE_{lin} for the linear fitting to the contact pressure calculated for a subset.

To find a threshold for the model fitting based approach, the first quartile, median, and third quartile of the goodness of the fit criteria SSE_{mod}, R^2_{mod} and RMSE_{mod} are calculated for different methods of robust fitting for the work-set. The results are given in the below table 4.

SSE_{mod}	R^2_{mod}	RMSE_{mod}
1.0e+07* [0.1743 0.4793 1.2426]	0.7609 0.8779 0.9365	276.6219 449.2120 697.3921

Table 4: First quartile, median and third quartile of the dispersion of systolic blood pressure and the goodness of the fit criteria SSE_{mod}, R^2_{mod} and RMSE_{mod} for the subset.

Table 5 shows the results of the categorization using different thresholds. The goodness of the fit parameters SSE_{mod}, R^2_{mod}, RMSE_{mod} and the number of rejected measurements are included.

4 Discussion and Conclusion

The first example, shown in Figure 8, indicates that the model fitting approach is working well and could be the right way to go. The data points already show a distinct shape and the fitting works well. In contrast, the data points in the second example are more scattered. The fitting does not work well in this case. This indicates that the quality of the measurements has a great influence on the quality of the fit.

The goodness of the fitted parameters, the R^2 in particular, also show a wide range. This also indicates that there are great differences in the quality of the fit for different measurements. Anyhow, the fitting works well for a part of the measurements, which is indicated by, e.g., the high third quartile of the R^2. Furthermore, this already indicates that the goodness of fit parameters, especially R^2, can be used to distinguish between good and bad measurements.

The results of the categorization of the measured data further support the above observations. Categorizing the measured data by the goodness of the fit of the linear polynomial fitting only leads to small improvements of the goodness of the model fitting although depending on the threshold already lots of measurements get excluded.

Method	Exclusion (linear)	Exclusion (model)	SSE_{mod}	R^2_{mod}	$RMSE_{mod}$	rejected measurements
-	-	-	1.0e+06* [19.63 47.93 117.43]	0.4549 0.7483 0.8866	281.6088 432.8869 677.1325	0
linear	$RMSE_{lin} \geq$ 3.1	-	1.0e+06* [1.4586 4.0650 8.6325]	0.5328 0.7825 0.8937	245.4182 412.7944 615.4822	183
linear	$RMSE_{lin} \geq$ 2.54	-	1.0e+06* [1.6480 4.3642 8.7856]	0.6331 0.8152 0.9064	249.9744 420.3820 626.3038	303
linear	$SSE_{lin} \geq$ 1.0e+4* 5.9620	-	1.0e+06* [1.4424 4.0421 8.4975]	0.5327 0.7853 0.8934	244.8690 411.6259 609.2378	188
linear	$R^2_{lin} \leq 0.9886$	-	1.0e+06* [1.4256 4.0168 8.4789]	0.5370 0.7879 0.8964	244.2957 410.2751 610.4114	198
model	-	$SSE_{mod} \geq$ 1.0e+07* 1.2426	1.0e+06* [1.4066 3.2432 6.0491]	0.5116 0.7740 0.8933	238.4647 356.4845 500.8422	107
model	-	$R^2_{mod} \leq 0.7609$	1.0e+06* [1.5425 3.9385 8.1521]	0.8314 0.8923 0.9337	259.8585 403.3576 603.6834	235
model	-	$R^2_{mod} \leq 0.8779$	1.0e+06* [1.3604 3.3716 7.4848]	0.9034 0.9279 0.9546	239.8867 371.3517 563.2087	324
model	-	$RMSE_{mod} \geq 697$	1.0e+06* [1.4127 3.3117 6.1229]	0.5069 0.7679 0.8935	238.9084 360.1372 509.4549	104

combined	$RMSE_{lin} \geq 3.1$	$R^2_{mod} \leq 0.8779$	1.0e+06* [1.4211 3.8300 7.4848]	0.9034 0.9282 0.9552	238.6218 396.8745 563.2087	364
combined	$RMSE_{lin} \geq 3.1$	$R^2_{mod} \leq 0.7609$	1.0e+06* [1.8223 3.9946 7.7939	0.8343 0.8921 0.9347	271.4662 412.8987 582.1261	305
combined	$RMSE_{lin} \geq 2.54$	$R^2_{mod} \leq 0.8779$	1.0e+06* [2.3574 4.2898 8.3234]	0.9035 0.9259 0.9514	301.0549 411.8377 602.5087	391
combined	$RMSE_{lin} \geq 2.54$	$R^2_{mod} \leq 0.7609$	1.0e+06* [2.1357 4.7765 8.0394]	0.8435 0.9011 0.9396	286.2074 431.9334 589.1964	363

Table 5: First quartile, median and third quartile of the goodness of the fit parameters SSE_{mod}, R^2_{mod} and $RMSE_{mod}$ for different methods and threshold for categorizing the measurements.

Categorizing with respect to the various goodness-of-the-fit-parameters of the model fitting leads to better results. Nevertheless, in some cases less then 100 of the 443 measurements would be accepted. The combination of the two categorization methods does not lead to a big difference compared to only using the goodness of the model fitting parameters as criterion. Overall, good results can be achieved when choosing the right criterion. The R^2 of the model fitting seems to be the best choice. However, it is necessary to find a balance between not excluding too many measurements and still obtaining good results.

To sum up, the model fitting works well for a part of the measurements, but not so good for a great part of the measurements. There are some indicators that this can be traced back to the quality of the measurements. Still, the approach itself shows great promise. Hence, before looking into the resulting absolute values for the systolic and diastolic blood pressure, more investigations on how to improve the fitting by filtering out bad measurements, increasing the measurement quality itself, or preprocessing the measured data is needed. Furthermore, at the same time the possibilities how to categorize the measurements into good and bad ones should be investigated further to find the right compromise between excluding and including measurements.

References

[1] Philipp Baumann. *Model-based Method for cuff-less blood pressure measurement using the oscillometric finger-pressing method* [master thesis]. Institute for Analysis and Scientific Computing. Technische Universitat Wien; 2020.

[2] *Stadium Shape* https://www.calculatorsoup.com/calculators/geometry-plane/stadium.php; accessed on 15.06.2022.

[3] Charles. F. Babbs. *Oscillometric measurement of systolic and diastolic blood pressures validated in a physiologic mathematical model*. BioMedical Engineering OnLine. 2012; 11. doi: 10.1186/1475-925X-11-56.

[4] Lachel Story. *Pathophysiology: a practical approach*. 3rd ed. Jones & Bartlett Learning; 2018.

[5] MathWork *Least-Squares Fitting* https://de.mathworks.com/help/curvefit/least-squares-fitting.html#bq_5kr9-9. Accessed on 23.01.2022.

Service-Oriented Architecture for Automatic Evaluation of Urban Logistical Concepts

Richard Pump[1], Lasse Bienzeisler[2], Torben Lelke[2], Volker Ahlers[1*], Arne Koschel [1]

[1]University of Applied Sciences and Arts Hannover, 30459 Hannover, Germany; *volker.ahlers@hs-hannover.de
[2]Technische Universität Braunschweig, Institute of Transportation and Urban Engineering, 38108 Braunschweig, Germany

Abstract. With the rapidly increasing availability of logistical concepts new tools are required to provide accurate estimations of concept effectiveness to urban planners. In this paper we describe a service-oriented architecture providing automated concept evaluation through agent-based traffic simulation, combining general traffic models with specialized logistical models into singular simulations. Key focus of the paper is the integration architecture utilized to combine the different tools from a previously developed manual workflow. The architecture is designed to incorporate multiple different tools into a combined workflow, providing non-domain users with a highly specialized tool.

Introduction

Urban logistics is currently changing at a rapid pace. An ever increasing consciousness for environmental factors, new regulatory measures, new services and a pandemic are moving populations from traditional solutions towards utilization of novel logistical concepts [1, 2]. This development confronts urban planners with new challenges as the number of design options for a city logistics system continues to increase, challenging the selection of the most suitable measures to improve the quality of urban mobility and thus environmental, economic, and social effects. New tools are needed to support decision making in municipal planning agencies to increase utilization and effectiveness of logistics solutions [3]. A team consisting of traffic engineers, business IT specialists, computer scientists, and munic-ipal government employees was tasked in the research project *USEfUL* to create a simulation-based decision support tool for urban logistics [4, 5].

An agent-based simulation approach using the multi-agent transport simulation (MATSim) [6] was chosen to evaluate the impacts of logistical concepts on urban traffic patterns within the city of Hannover. For the evaluation, different key performance indicators (KPIs) were defined. Based on these simulation results, the observed impacts on the KPIs were evaluated in order to derive recommendations for urban planners. Consequently a hand-crafted traffic model [7], adapted to the resulting needs and behavioral patterns stemming from logistical concepts was developed, which in turn fed a semi-automated evaluation tool chain. Due to the comparatively long run times of the agent-based simulations and the high computational effort, all scenarios were simulated manually and only the corresponding impacts were stored in the tool. These results are on display on the project's web page [8], where users can gather information about the concepts, the evaluation areas and predicted effects on different KPIs.

However, the workflow with the semi-automatic traffic model generation and the evaluation framework is currently only applicable to the city of Hannover. In particular, the setup of the traffic model is limited by available data sources and therefore not directly transferable to other cities and municipalities. To provide similar assistance to other communities, a completely automated architecture needs to be designed and implemented. The resulting tool has to utilize public and private data sources to create an accurate baseline model of the area of interest, before standardized changes to the model implement novel logistical concepts.

To tackle these issues – and increase the usefulness of the web-based tool – the follow-up project *USEfUL-XT* aims to increase the transferability of the *USEfUL* workflow. In this paper we present the architecture to

combine previously manual workflows using a service-oriented approach. A high-level view of the different services is given, as the implementation of the services is still in progress. The result is the concept of an integrated, service-oriented and cloud-based framework capable of automatically collecting and processing the required data, creating a simulation model and performing the resulting simulation runs. As the specified simulation scenario only need to be simulated once, the computation needs are also dynamic and efficient resource usage demands a dynamically scalable solution with adequate storage space to store results.

Section 1 will give an overview of related work. In the following section 2 the current workflow of the project is presented, which is then expanded to an automatic workflow in section 3. Remaining challenges are discussed in section 4 and a conclusion is given in section 5.

1 Related Work

A similar tool to the *USEfUL* web application was provided by [9]. The Urban Transport Roadmap provides statistical evaluations for many regulatory measures and estimates the impacts of technological development on urban traffic. However, the tool focuses on very rough estimates for many different cities and allows in-depth analysis of combinations of measures.

Another theoretical framework for automated evaluation of urban traffic was proposed by [10]. In their proposed system, a user can utilize a partially automated co-creation process to construct simulation models of a city. After model creation, partial changes to the model are proposed to the user, which, when chosen, are in turn simulated within multiple simulation tools. At the same time a rule-based system watches the simulation for inconsistencies and provides input to the user to correct these. The publication focuses on the process of creating the tool, rather than the tool itself. It is unclear if the tool can provide automated model creation for multiple areas and logistical concepts. Furthermore, the proposed system of [10] does not include an expert system to fast-track concept evaluation. The proposed system remains theoretical.

In another work, [11] present a generalized pipeline for the generation of agent-based transport models in France. This pipeline presents a standardized approach for processing data sources to synthesize a synthetic population and assign mobility behaviour to the agents.

The paper also includes a detailed validation of the method. However, the described method is focused entirely on the generation of a model for private traffic omitting commercial traffic and is adapted to the specifically in France available data.

An example for a microscopic modeling approach for commercial traffic is presented in [12]. Therein, the authors then employ land use and structural data to generate businesses and the respective employees and vehicle fleets. By applying the German commercial travel survey, each vehicle is equipped with a daily schedule.

Meanwhile, many other simulation models and studies have been created to identify issues and solutions for urban logistics [13]. However, model creation was not completely automated and often only small areas of urban logistics were modelled. Our proposed system approaches urban logistics from a more abstract point of view, allowing a rough estimation of impacts for many concepts and areas, through automated model creation, simulation and evaluation.

2 Current Solution

The current workflow combines manual data collection, preparation, and model calibration as well as simulation and evaluation. A lightweight, web-based decision support tool was created, not slowed down by long simulation run times, as users want to use the tool at a quick glance. The goal of the process was the easy-to-understand representation of logistic concept impacts on specific KPIs, which are presented to users in a web-based decision support tool. Traffic and logistic simulations are performed using MATSim to benchmark the impact of new logistical concepts. The process can be split into seven parts, as shown in Figure 1.

The first step of the workflow is data collection, as many different sources of information have to be utilized to manually collect the necessary traffic supply and demand information. Several open data sources like OpenStreetMap (OSM) and public transport providers are considered to create a road network with an integrated public transport system for the traffic supply needed in the MATSim model.

To generate a realistic traffic demand, multiple studies and non-public data from companies and municipalities are consolidated into a synthetic population. Furthermore, different input surveys are used to derive the travel or logistic demand from the synthetic population. From the collected data a *basecase* model is created,
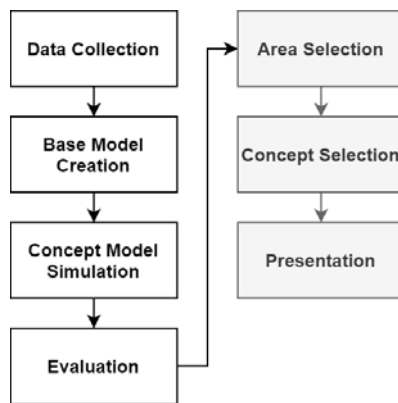
Figure 1: Current manual workflow of the project *USEfUL*. User interactive parts marked in grey.

Figure 2: Planned workflow for the *USEfUL*-Application. User interactive parts marked in grey.

representing the status quo of traffic within the research area. A manual calibration of the model using traffic counts, as well as a validation against different mobility parameters is performed to achieve a high model accuracy. Building upon the previously created *basecase*, demand changes due to the implementation of novel logistic concepts are replicated in the model and need to be simulated subsequently. Each concept is parameterized in different dimensions (e.g. usage of electric vehicles, total acceptance percentage, etc.), studying concepts more in-depth. A large amount of simulation runs were needed for every area of interest and each parameter combination, since multiple logistical concepts were compared to provide a useful decision support.

Simulation results are in turn evaluated with regards to eight KPIs: acceptance, emissions, area usage, costs, implementation potential, traffic impacts, economic feasibility, ecological break-even-point. For the evaluation, the *basecase* is considered as the starting point and trends on the KPIs through utilization of logistic concepts are derived. After all possible scenarios are simulated, evaluation data is combined in a database queryable through a web-application. Users can now select a research area, a concept (possibly modify it through parameters) and are presented with the evaluated simulation results.

While this workflow produces good results for pre-defined areas, adaption to new areas is labor intensive and slow, diminishing the usefulness for other parties. Furthermore, since all possible combinations of areas, concepts and parameters need to be simulated a priori, timely simulation requires a large amount of computational resources. A optimized process would allow the
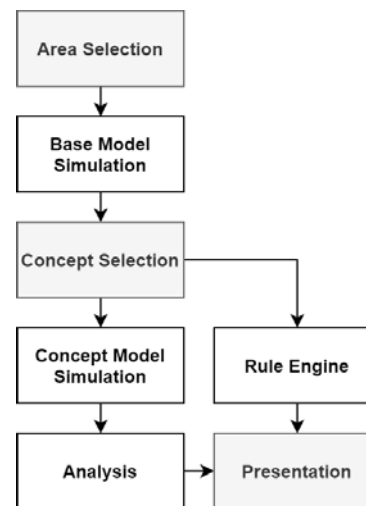
users to select the area of interest, a specific concept and then receive the simulation results on-demand (either through a new simulation study or previously performed simulations). Consequently, we designed this concept of an automated simulation framework. This goal-process is shown in Figure 2.

The improved workflow also utilizes a rule-based expert-system to give impact estimations almost instantly, as opposed to the simulation, where turnaround times of multiple days, if not weeks are to be expected. To achieve this workflow, major challenges must be solved, most importantly the automatic creation of models based on automatically collected data. While the previous process already uses automated tools at each step in the workflow, data transfer between steps was handled manually, increasing the total time needed. Implementing the new workflow requires a clear definition of software interfaces, processes and deployment into an easily scalable environment.

3 Service-Oriented Cloud-Based Workflow

Service orientation and cloud usage are computing patterns that address multiple issues also encountered in the simulation workflow of *USEfUL*. Service orientation allows the easy integration of quickly evolving tools into combined workflows while providing abstract interfaces, decoupling different steps of software processes [14]. This in turn allows the easy combination
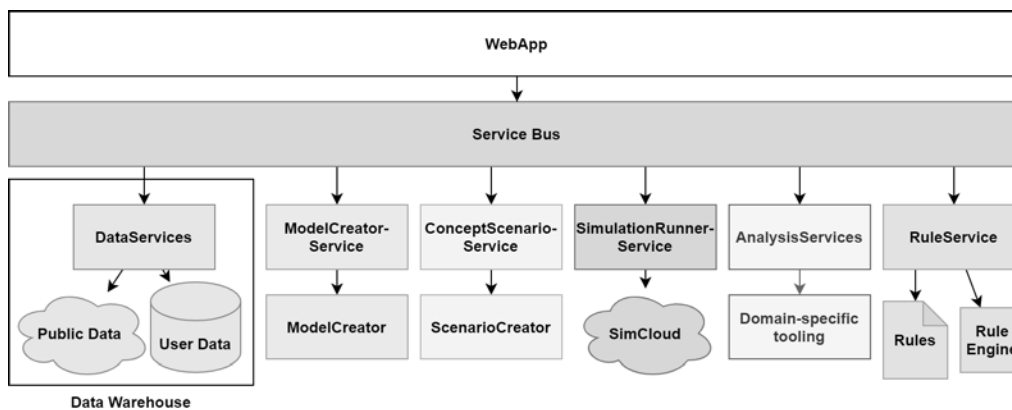
Figure 3: Proposed Architecture for the system. Each step of the previous workflow of the project is encapsulated into a service, which can be invoked in order from the user-accessible web-application

of many different software tools into a combined application. Cloud-based computing provides quickly scalable infrastructure by combining different applications on the same hardware, therefore reducing the cost for hosting of applications.

With a cloud-based simulation service, users can request simulations ad-hoc, paying only for the computational power that is actually needed to run the simulation, instead of investing in expensive simulation hardware. Since primary user groups are located in communal administration and other non-software firms, this approach increases the attractiveness of the solution to the end user. while the architecture is aimed at a cloud deployment, it is not necessary to rely upon an external cloud provider. Through the usage of a private cloud, the entire software can run on-premise, if e.g. data security or privacy requirements dictate it. In general service-orientation is implemented by encapsulating specific tasks of the workflow into independent services that can be recombined for other workflows. Figure 3 shows the proposed service-oriented architecture for the automated solution.

The workflow of the proposed system is controlled by the already existing WEBAPP, providing user interaction and service orchestration. Since only a single workflow – the evaluation of logistic scenarios – is to be expected, a flexible workflow engine is not necessarily needed and implementation complexity can be reduced. In case the workflow changes for the different simulations, an increased workload to implement the changes is to be expected, but does not outweigh the reduction of implementation complexity. As the WEBAPP has already been developed in *USEfUL*, it can

easily be adapted to the necessary changes.

The SERVICE BUS provides stable service endpoints for usage through the WEBAPP (or other applications) and connects them to the service implementations. This effectively decouples declaration and definition of different tasks, allowing easy redevelopment of different parts of the overall workflow without leading to widespread changes. Many different existing solutions can be adapted for this particular purpose. Communication between the SERVICE BUS and other components is technology-dependent and can be implemented in multiple different ways. As the chosen simulation tool MATSim utilizes xml-files for configuration and modelling, data transfers will also utilize the xml-standard to achieve design homogeneity.

The SERVICES implement the steps of the workflow and utilize technologies independent of the rest of the application. This allows technology selection according to the domain-specific needs, as well as flexibility when services are updated to new methods. A description of the services is given in the following sections.

Some cross-cutting concerns are life cycle management and security, as these are needed at all levels of the application. While life-cycle management needs to be decentralized due to the technical nature of the domain, security can be handled at the SERVICE BUS and deployment environment. E.g. access to services from external sources can be blocked by a firewall and internal compartmentalization is achieved by extending the existing role-based-access-control to service bus level.
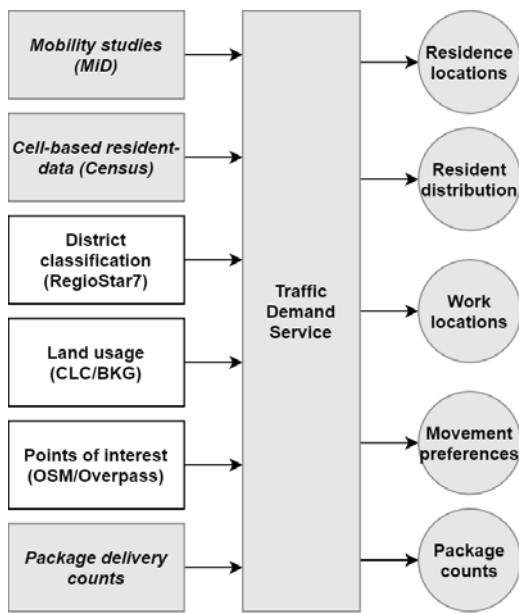
Figure 4: High-level view of the Demand data service. White background marks machine readable sources, slanted writing marks manually interpreted Data.

3.1 DataServices

The data services, are responsible of adapting different sources of data into the system. To create simulation models for urban logistics, different information sources are summarized to create the traffic supply as well as the traffic demand.

As these data sets are built from many different sources, the services are responsible for aggregating this data and providing the necessary information in a standardized format. The data services consolidate the processed data in a data warehouse and allocate it to the associated services for further processing. While some data might be pulled from standardized web services, other need to be manually interpreted, prepared and provided in a suitable format. Consequently most of the technical and logical complexity of handling different data is localized in these services.

Figure 4 shows a high-level view of one of the main data services, the TRAFFIC DEMAND SERVICE. This Service is responsible for providing information about traffic demand and population behavior, which in turn is used to generate traffic demand within the MODELCREATORSERVICE. Information for this service is gathered from public APIs like OSM/Overpass, public statistical data, manually extracted from documents, and non-public studies. Data pulled from public APIs

can easily be converted into the necessary XML structure, utilized by consuming services. Other Data, like the aforementioned public statistical data, needs manual conversion and own storage infrastructure, as document structures vary vastly between different sources or iterations of the same studies. For example, the study *Mobility in Germany 2017* added a new excel-based tool for data exploration, which was not available for the studies predecessor, created in 2008 [15]. While automatic extraction of the study is possible, the created tool would only work for this iteration of the study. The resulting effort/effect-balance is not favourable for automation. To make manually extracted data available for the automatic workflow, it is entered into a database, which provides a machine readable data format. Since the TRAFFIC DEMAND SERVICE collects data from different sources and provides a unified interface for consumers, it can be viewed as a data warehouse.

As part of the modelling process, the traffic demand service also provides data for the automated model calibration service. Thus, mode share information of the simulation area as well as other mobility parameters must be specified and provided by the user. An essential element for the quality of the model is the availability of real traffic data from the simulation area particularly consisting of vehicle count data of different sections of the network. While this detector data can be accessed online for specific network connections, it is often not directly available. Therefore, this missing component must be provided by the user.

3.2 ModelCreatorService

After all necessary input data is collected and processed into the data warehouse, the MODELCREATORSERVICE is executed. This service contains three consecutive modeling steps that gradually generate an agent-based transport model for individual traffic along with a service-based model for commercial traffic (Figure 5).

In the first step, a synthetic population consisting of households with corresponding agents is generated based on the grid cells that are deposited in the data warehouse. Grid cells are selected according to the area of interest included in the execution request. Each of the agents in the population represents one person living in the specific cell and is assigned with certain socio-demographic attributes, such as gender or age, as well as attributes that impact the mobility, such as the possession of a driving licence or public transport ticket. In addition to these agents, companies are synthesized as
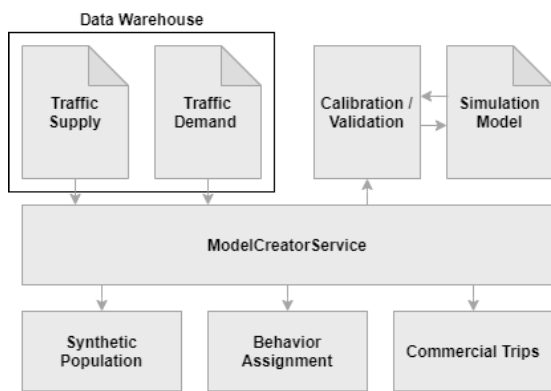
Figure 5: Architecture of the ModelCreatorService

location for work activities and as instances that generate commercial or logistic traffic. The companies are differentiated by industry sectors and also obtain attributes such as the number of vehicles and the number of agents working at that location.

In the second step of the model creation, each agent is assigned a mobility behavior corresponding to the predefined attributes. The behavior is defined by a sequence of activities the agent performs during a day and the necessary trips that the agent must perform to reach those activities. These patterns are provided by the data services and also contain additional information such as the transportation modes used and the travel distance for the trips. The location choice for the activities is then carried out on the basis of these information along with land-use data.

The last element of the MODELCREATORSERVICE is the generation of commercial trips. In this process, the defined vehicles for each company are assigned with a sequence of services they have to operate on the simulated day. The services act in a similar way to the activities of the agents and are linked to the population and other companies. For example, if a craftsman performs a service for an agent, the agent has to be at home. A special focus is laid on logistical aspects of the model. Specifically, the parcel demand is used to generate service sequences for parcel delivery vehicles of multiple delivery services. The resulting vehicle routing problem is solved using a ruin-and-recreate-algorithm and resulting trips are assigned to the vehicles [16]. The output of the MODELCREATORSERVICE consists of several independent XML-files, representing the model in its entirety. This model then has to be calibrated and validated using additional data sources from the warehouse that were not used for the model creation.
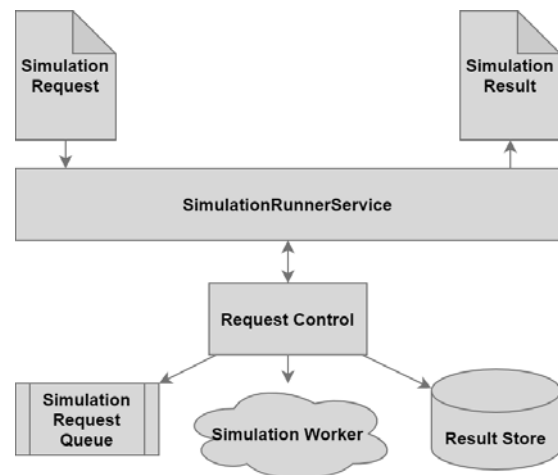

Figure 6: Simulation Runner Service responsible for asynchronous execution of simulation requests.

3.3 ConceptScenarioService

After the *basecase* has been created, further changes to the model are necessary to inspect different logistical concepts. In the CONCEPTSCENARIOSERVICE subcomponents make changes to the model according to the concepts. For example, some of the traffic resulting from grocery runs is replaced by a centralized grocery distribution system. To add a new concept, new components can easily be added to the service, without changing other parts of the system. Since the logistical concepts are not in service at the research area, validation of the changed model proves difficult.

3.4 SimulationRunnerService

The simulation service is responsible for scheduling and executing the simulations. A detailed analysis through simulations can be provided by utilizing a worker cloud where simulation tasks can be asynchronously executed.

As shown in Figure 6, SIMULATION REQUESTS are accepted by the SIMULATIONRUNNERSERVICE, where they can be stored in a queue until resources are available for execution. The SIMULATION REQUEST contains XML-Files which were generated in the MODELCREATORSERVICE along with configuration parameters for the simulation, which have to be provided by the user. Data is then fed into the SIMULATION WORKERS, which execute MATSim simulations on dynamically scaling infrastructure e.g. through the use of Docker containers. After the simulation runs are finished, data is pushed into a RESULT STORE for sub-

sequent requests to prevent repeated simulation of the same model/parameter-combination.

3.5 AnalysisServices

The final step before presenting concept impacts to the user is the analysis of simulation results. The analysis is carried out by applying models for different KPIs to parts of the simulation output (e.g. additional traffic caused by the given concept). As models are created by domain experts, an integration for widely used tools like Microsoft Excel is required. The different models compare information from the simulation of the modified models to the *basecase* and derive trends for KPIs. This allows the easy-to-understand representation in the final visualization for the user.

One example of ANALYSISSERVICES is the AREA MODEL, which gives an estimation on the expected change of area needed for the implementation of a given logistical concepts. The AREA MODEL uses information like the amount and type of delivery vehicle used to implement a given concepts and then calculates additional area needs for e.g. construction of micro hubs. This is in turn compared to the reduction of e.g. parking spaces to calculate the net difference. Since the effects of concepts are also interconnected, the AREA MODEL feeds its result directly into the COST MODEL, which predicts cost changes.

3.6 RuleService

As an alternative to the time-consuming simulation path (shown in Figure 2), a rule-based expert system can be utilized to estimate the impacts KPIs. The RULE-SERVICE uses the JSONRULESENGINE and multiple sets of Rules to estimate Results, as each concept reacts differently to structural and behavioural peculiarities of different concepts. While not providing the accuracy achieved by the simulations, the RULESERVICE allows the preliminary study of concepts effects on non-simulated areas to identify promising combinations for further study.

The rules are built upon previous simulation results for each logistical concept and model the connection between concept effects and structural attributes of areas. As no high accuracy is expected until a large amount of simulations have been carried out, the first iteration of the rules engine only predicts three categories of change, instead of a numerical scale. As more and

more simulations are carried out, new results are incorporated into the rules, thus improving model prediction. However, the rule engine cannot predict changes in radically new areas or for unknown logistical concepts.

3.7 WebApp

After the impacts of the concept have been evaluated, a web-based decision support tool presents the results to the user. This WEBAPP is built upon Laravel [17], using a modern design to attract users. It uses a rule-based expert system [18]. Functionalities for selecting areas and concepts as well as dynamical presentation of results are already implemented, therefore only additions to existing components are necessary.

4 Remaining Challenges

While the technical integration of all existing tools can easily be achieved through the use of available software solutions, some procedural issues remain. First and foremost the validation of the simulation models remains problematic, as multiple data sources for similar information are required. Data has proven to be relatively scarce, as privacy of residents or workers needs to be protected and some data are simply not collected. Furthermore, validation is currently a time-consuming, manual process, that has not been fully automated yet.

Another challenge is the calibration of the simulation models, as this is again a manual process, requiring a human-in-the-loop approach to properly interpret information and adapt parameters accordingly. An automated process could involve a meta-optimization approach such as evolutionary algorithms, but would in turn increase resource demand and runtime. Since open data projects are utilized, data quality is inconsistent, as data tends to be biased. One of the main reasons for this are the inhomogeneous contribution patterns of its contributors [19]. This issue is not fixable through the proposed system, as automatic data quality improvement is out of scope for its requirements.

5 Conclusion

In this paper an architecture for the automation of simulation and decision support has been presented. Built upon a previously developed workflow, the system aims to allow users to evaluate novel logistical concepts in specific research areas. The system shall provide rough

estimates on effects on key performance indicators of traffic like emissions and population behaviour. This allows users to evaluate logistical concepts in theory and aids in preliminary selection, reducing the need for cost-intensive prototype-projects in the real world.

While the technical aspects of the proposed system do not pose show-stopping challenges, domain specific workflows, like simulation validation need to be developed further to implement the system. In future work a prototypical implementation as well as the definition and evaluation of automated processes for simulation validation and calibration are planned.

Acknowledgement

References

[1] Kunze O. Replicators, Ground Drones and Crowd Logistics A Vision of Urban Logistics in the Year 2030. *Transportation Research Procedia*. 2016;19:286–299. Transforming Urban Mobility. mobil.TUM 2016. International Scientific Conference on Mobility and Transport. Conference Proceedings.

[2] Dablanc L. E-commerce trends and implications for urban logistics. *Urban logistics Management, policy and innovation in a rapidly changing environment*. 2019;pp. 167–195.

[3] Lagorio A, Pinto R, Golini R. Research in urban logistics: a systematic literature review. *International Journal of Physical Distribution & Logistics Management*. 2016;46:908–931.

[4] Pump R, Gohe S, Trott M, auf der Landwehr M, Koschel A, Ahlers V, Gusig L, von Viebahn C. Towards Extending USEfUL-ness for Urban Logistics with Service-orientation. In: *SERVICE COMPUTATION 2021*, SERVICE COMPUTATION, International Conferences on Advanced Service Computing. Porto, Portugal: IARIA. 2021; pp. 13–19.

[5] Bienzeisler L, Lelke T, Wage O, Huck LM, Friedrich B. Uncertainty and Variability Analysis of Agent-Based Transport Models. *Transportation Research Procedia*. 2022;62:719–726.

[6] Horni A, Nagel K, Axhausen K, eds. *Multi-Agent Transport Simulation MATSim*. London: Ubiquity Press. 2016.

[7] Bienzeisler L, Lelke T, Wage O, Thiel F, Friedrich B. Development of an Agent-Based Transport Model for the City of Hanover Using Empirical Mobility Data and Data Fusion. *Transportation Research Procedia*. 2020; 47:99–106.

[8] Initiative Urbane Logistik Hannover. USEfUL. https://useful.uni-hannover.de/.

[9] de Stasio C, Fiorello D, Fermi F, Martino A, Hitchcock G, Kollamthodi S. On-line Tool for the Assessment of Sustainable Urban Transport Policies. *Transportation Research Procedia*. 2016;14:3189–3198. Transport Research Arena TRA2016.

[10] Dossou PE, Vermersch A. Development of a decision support tool for sustainable urban logistics optimization. *Procedia Computer Science*. 2021;184:476–483. The 12th International Conference on Ambient Systems, Networks and Technologies (ANT) / The 4th International Conference on Emerging Data and Industry 4.0 (EDI40) / Affiliated Workshops.

[11] Hörl S, Balac M. Synthetic population and travel demand for Paris and Île-de-France based on open and publicly available data. *Transportation Research Part C: Emerging Technologies*. 2021;130:103291.

[12] Reiffer A, Heilig M, Kagerbauer M, Vortisch P. Microscopic Demand Modeling of Urban and Regional Commercial Transport. *Procedia Computer Science*. 2018;130:667–674.

[13] Jlassi S, Tamayo S, Gaudron A. Simulation Applied to Urban Logistics: A State of the Art. In: *City Logistics 3*. John Wiley & Sons, Ltd. 2018; pp. 65–87.

[14] Rosen M, Lublinsky B, Smith KT, Balcer MJ. *Applied SOA: service-oriented architecture and design strategies*. John Wiley & Sons. 2012.

[15] Mobilität in Deutschland 2017. https://www.mobilitaet-in-deutschland.de/archive/publikationen2017.html.

[16] Zilske M, Joubert JW. Freight Traffic. In: *The Multi-Agent Transport Simulation MATSim*, edited by Horni A, pp. 155–156. Ubiquity Press. 2016;.

[17] Laravel. https://laravel.com/.

[18] Heumann M, Pump R, Breitner MH, Koschel A, Ahlers V. Towards Sustainable Transport: A Strategic Decision Support System for Urban Logistics Operations. *Innovation Through Information Systems*. 2021;pp. 367–381.

[19] Basiri A, Haklay M, Foody G, Mooney P. Crowdsourced geospatial data quality: challenges and future directions. *International Journal of Geographical Information Science*. 2019;33(8):1588–1593.

Raising Awareness of Climate Change Impact and Mitigation – The *MyWorld* Simulation Game

Uwe Beyer, Magdalena Karnassnigg, Oliver Ullrich

Fraunhofer Institute for Intelligent Analysis and Information Systems IAIS, Schloss Birlinghoven, 53757 Sankt Augustin, Germany; *uwe.beyer|magdalena.karnassnigg|oliver.ullrich@iais.fraunhofer.de*

Abstract. As climate change increasingly impacts natural systems and living conditions all over the world, it becomes even more important that members of the public understand the probable course of climate change, its impact on world-wide and local ecology and living conditions, and the extent to which mitigation measures can alleviate that impact. Researchers can contribute to this by developing simulation models of the course and impacts of climate change, and make them available to the general public, packaged with a user-friendly interface and progressively detailed information.

This paper introduces *MyWorld*, a simulation-based game that enables the player to experience the course and impact of climate change and to experiment with potential mitigation measures. The freely available game aims at facilitating a better understanding of the probable progression of climate change and its impact on living conditions in the world in general and specific countries in detail.

Introduction

Climate change increasingly impacts all areas of human existence, including such diverse fields as urban infrastructure systems and housing [1], century-old cultural heritage assets [2][3], medicine and human health [4], and agriculture [5]. With the range and velocity of climate change increasing, it becomes even more important that the general public understands its impacts and potential remedies.

Here, simulation can help. Wrapped in a user-friendly game-like environment, a (simplified) simulation model of global climate change and its impacts on living conditions, broken down to a user's local environment and extended by estimates of the effectivness of mitigation measures, can increase the awareness of changes ahead and improve decision quality regarding potential changes in economy, societal organization, and personal lifestyle. To reach those goals, a model does not have to be as precise as an analytical simulation for the validation of real-world decisions and strategies. In return, players have no patience to wait for hours for the conclusion of a simulation run – an underlying simulation model has to be fast, even at the cost of precision.

This paper presents the *MyWorld* simulation-based game [6] aimed at facilitating a better understanding of the probable progression of climate change and its impact on living conditions in the world in general and specific countries in detail, as well as the effect of potential mitigation measures on those living conditions. The game presents the players with a visualisation of the course of climate change in any specific country, gives them the opportunity to experiment with mitigation measures, and simulates the impact of those measures on the CO_2 balance and the further course of climate change itself. Playing the game thereby raises awareness of climate change impacts, potential mitigation measures and their effects and interdependencies.

Literature describes a number of serious games in the area of climate change and sustainability (for an overview, see Stanitsas et al. [7] or Gerber et al. [8]). Only a minority of approx. 10 % of those primarily aim at raising awareness [8], many of the others are more oriented towards strategy design [9], collecting data [10][11], or direct behavioral change [12]. Some are table-top games without computer support [9][13][14][15], while others are at least partially computer-supported [10][12][16][17][18][19][20]. Many of those examine specific (sub-)systems, like water management [17][19], household energy efficiency [12], and cultural heritage protection [20].

A few of these serious games warrant a closer examination: Van Pelt, et al. [17] describe a simulation-based game aimed at conveying the inherent uncertainties of climate change in the area of water management to expert stakeholders; their experimental setup includes ex ante and ex post surveys and control groups. They conclude that simulation-based games can be valuable in supporting the communication of climate change uncertainties.

The game proposed by Gangollels, et al. [12] aims at facilitating behavioral change in the area of household energy conservation, specifically at affordable housing communities. Based on their observations, they identify a significant potential for greenhouse gas savings that could be realised by individual behavior change. They propose to facilitate that behavior change by exposing members of the general public to a simulation-based game.

Bontchev, et al. [20] examine, based on the example of their own computer-based game, what factors robustly contribute to the awareness of climate resilience, especially in the area of built heritage sustainability. They find that learnability factors, e.g., ease of understanding the mechanics and gameplay, consistency in its mechanics, and direct feedback to a player's actions, contribute strongly.

De Kraker, et al. [19] propose the usage of a multi-player game to foster social learning, based on an example of river water management. They find that the game facilitates a convergence of perspective in stakeholders from various backgrounds especially if the simulation model's mechanics and intermediate computational results – and therefore, by extension, the underlying interdependencies of the real-world system – are clearly communicated and not hid as a black box.

Based on that – admittedly, non-comprehensive – literature review, there seems to be a research gap regarding an awareness-raising game that covers the whole climate system and allows players to experiment with the impact of mitigation measures as they are discussed in politics and media. The review also showed that a simulation-based game should be clear about the underlying model's mechanics, should contain information on any sub-system and parameter that can be accessed by a player if they desire so, and should expose the player to direct feedback regarding every decision they make. The *MyWorld* game aims to fill that gap.

The paper continues with a short introduction to the *MyWorld* game as seen by the user (Section 1), followed by a description of the underlying simulation model (Section 2). It concludes with some thoughts on the context the game can be used in and an outlook on further research (Section 3).

1 The *MyWorld* Game

MyWorld offers a number of main views on the developments and dependencies of the underlying climate change model; it tries to convey to the user a sense of what those developments might actually mean to them and their local context. The main views are a world map and country information, a local and global 'climate press', the CO2 balance of the world or specific countries, and the mitigation measures selected by the user. While aimed at being easily understood by novice users, *MyWorld* also puts a focus on offering detailed information on all aspects of climate change.

The game can be downloaded freely from its web site [6].

1.1 World Map and Country Information

The first major view depicts a world map on which the player can select a country. Detailed data on that country will be shown in the country data area on the right of the map (see Figure 1). A date slider enables the player to select a year – between 1960 and 2100 – for that they would like to examine data. Beneath the data slider an info area depicts in what years, given the current set of parameters and mitigation measures, the model estimates that global temperature will break the 2 °C, 3 °C, 4 °C, and 6 °C thresholds.

The country data area provides a wide range of both world-wide and country-specific data for a selected year, including population data, CO2 emitters, energy production, societal and humanitarian factors, climate- and weather-related data, ecologic and economic data. Each of these items provides an information button revealing progressively more detailed information of the parameter and the underlying interdependencies, and a thumbnail-sized graph that depicts its development over time. The graphs can be expanded for each variable for closer examination.

1.2 Climate Press

To increase the degree of immersion and to give a better understanding of course and impact of climate change as well as the effect of mitigation measure, *MyWorld* includes a 'simulation' of both local and regional press articles. These 'articles', for any combination of simulation time, selected country, and selected mitigation measures, give a summary of current developments world-wide or. Technically, these 'articles' are composed out of simple boilerplate text modules based on the current development of the simulated climate and living conditions at any point in simulation time.
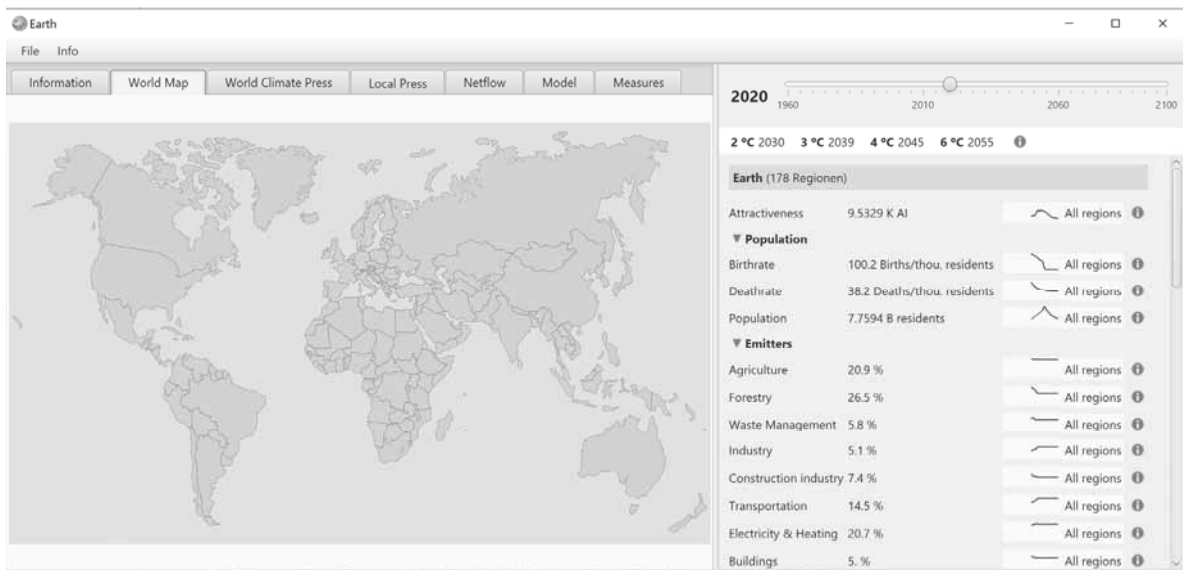
Figure 1: A screenshot of *MyWorld* showing a world map with the active country (left, Austria), a date slider (right at the top) and a number of world-wide and country-specific data points (right, bottom) regarding the active country at the specified point in time.

This is a significantly shortened example of the 'news article' localized for Germany for the year 2030 with some activated mitigation measures:

"Germany wants to be climate neutral by 2045 – By 2039, a 75 % reduction is targeted. Food and tabacco industry, chemical industries, agriculture and livestock, and cement manufacturing will be equipped with filters for carbon capture and storage of 75% of all emissions. Power generation will be CO2eq-free by 75%, with at least 901 TWh CO2eq-free energy generated. For this purpose, at least 128,742 wind turbines or 64 nuclear power plants are required. The purchasing power of the population will be reduced by 5.8%."

1.3 CO2 Balance

For each point in simulation time, as indicated with the date slider, the game depicts the CO2 balance resulting from the currently simulated climate system, including the mitigation measures selected by the user (see Figure 3). *MyWorld* distinguishes between all major carbon sources and sinks, including oceanic CO2 uptake, human-caused emissions and carbon capture and storage (CCS), photosynthesis, freshwater, weathering, vulcanic eruptions, as well as other natural sources. The game also summarizes whether the CO2 level in the atmosphere under the given conditions is growing or shrinking, i.e., whether the mitigation measures selected by the user are sufficient to stop climate change in the long run.
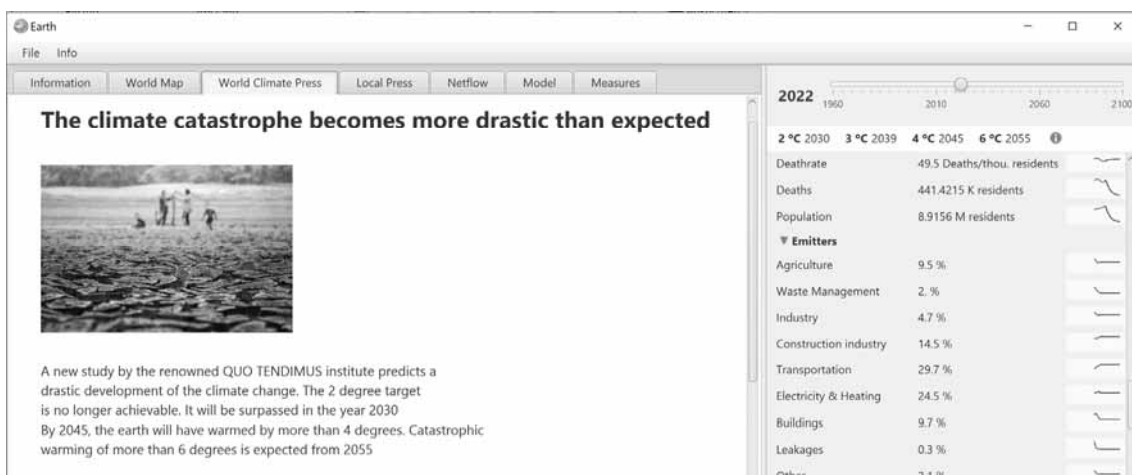

Figure 2: *MyWorld* offers both word-wide and local 'news articles' regarding the course and impact of climate change and the effect of user-selected mitigation measures.
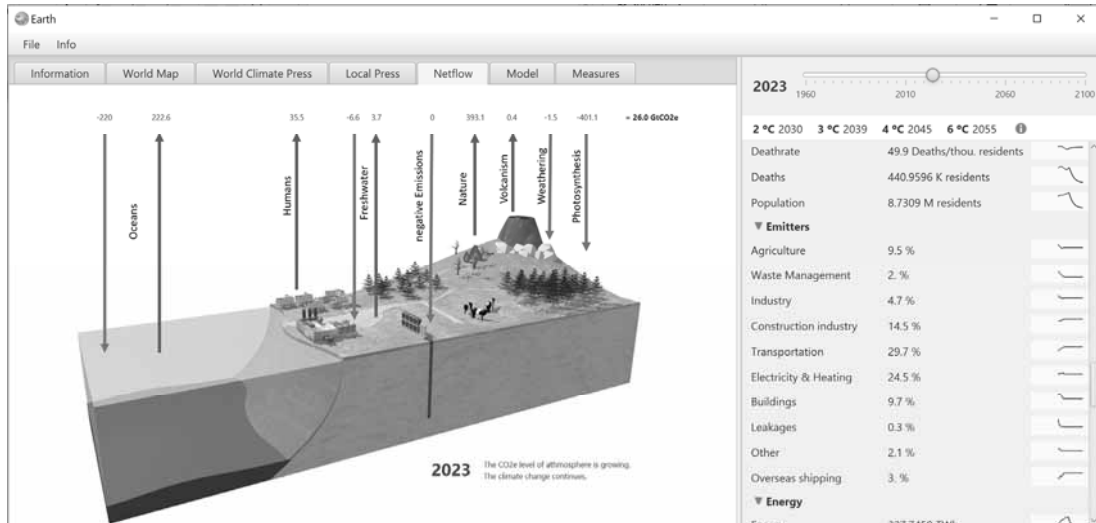
Figure 3: A screenshot of *MyWorld* showing the flow of CO2 equivalents for a selected country and point in time as a sum of the flows to and from, among others, the oceans, human activities, freshwater, photosynthesis, and CCS activities.

1.4 Mitigation Measures

MyWorld offers its users the opportunity to define and implement mitigation measures at any point in simulation time and enables them to investigate how these measures might influence the further course of the earth's climate. As a starting point for tinkering, the model presets the measures that various nations agreed upon as part of their Nationally Determined Contributions (NDCs). To be easily understood, measures form English sentences, e.g., "For Australia, phase out CO2e down to 0.1 times the value of 1990 by the year 2040, starting in 2025."

2 The *MyWorld* Simulation Model

To be of use in a near real-time game environment, the simulation model has to be executed fast, therefore putting limits on its complexity and preciseness. Simplifications are justifiable, as the model is not aiming at evaluating real-world decisions and strategies for their effectiveness and efficiency, but to give the user an impression on what impact climate change might have on their living conditions, and what effect mitigation measures might have on the further course of climate change.
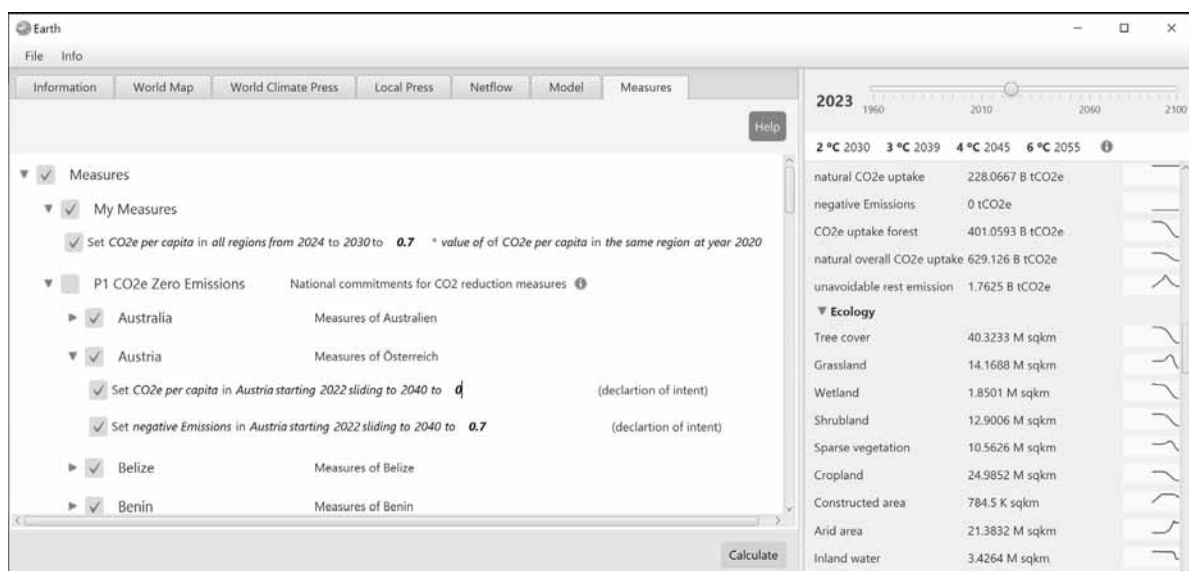

Figure 4: A user can define mitigation measure by selecting a country (or the world) and composing the elements of an English sentence from text elements. An example would be: "For Australia, phase out CO2e down to 0.1 times the value of 1990 by the year 2040, starting in 2025."

The following sections first describe the sources of the utilized data, then the basic simulation model based on a set of difference equations [21][22], and finally details the way potential mitigation measures selected by the user are integrated with the calculations.

2.1 Data and Constant Sources

For the *MyWorld* climate model, only data and constants from reputable data sources such as the UN, IPCC, WorldBank, or Our World in Data, are used. A separate view enumerates the sources of all data, including where to find them on the internet (see Figure 5). As with most complex models, experts disagree on some of the constants, such as certain demographic indicators. These constants can be adjusted by the player to suit their needs. The following paragraphs exemplarily describe some of the most important data series, their sources, and the way of integration with the *MyWorld* model.

The **CO2e-level** in the atmosphere is continuously measured by NOAA [23]. CO2e stands for "CO2 equivalents" and contains the greenhouse gases listed by the International Panel on Climate Change (IPCC) [24], primarily water vapour (H_2O), carbon dioxide (CO_2), methane (CH_4), nitrous oxide (N_2O) and ozone (O_3) as well as entirely human-made greenhouse gases, such as halocarbons and other chlorine- and bromine-containing substances, like sulphur hexafluoride (SF_6), hydrofluorocarbons (HFCs), and perfluorocarbons (PFCs).

Data on the **energy mix** per world region is collected by Our World in Data [25], albeit incompletely. Some of the data series show erratic trends, which is due to the fact that the data sets are incomplete. *MyWorld* estimates the future energy demand of a nation based on the current energy consumption per inhabitant. This method is inherently inaccurate as it does not take into account whether energy consumption per capita will increase or decrease. The current trends are diverging for different nations, so that an exact prediction seems hardly possible.

Current and future **population numbers and birth rates** per region are estimated by the UN Department of Economic and Social Affairs [26]. While the estimates by principle cannot be exact, the UN data collection is generally seen as the most reliable available.

Types of landscapes, especially percentage of **tree cover**, are monitored by the OECD [27]. *MyWorld* models changes in land cover as a simple function of deviation of temperature to the historical mean. This approach is very simplistic because it does not consider geography, global flow systems, or peculiarities of different nations. Predictions on local levels can therefore be inaccurate.

2.2 Basic Model

Climate change will have a significant – potentially devastating – impact on future living conditions. That said, the authors of the game want to avoid *MyWorld* presenting an overly pessimistic view of the future.
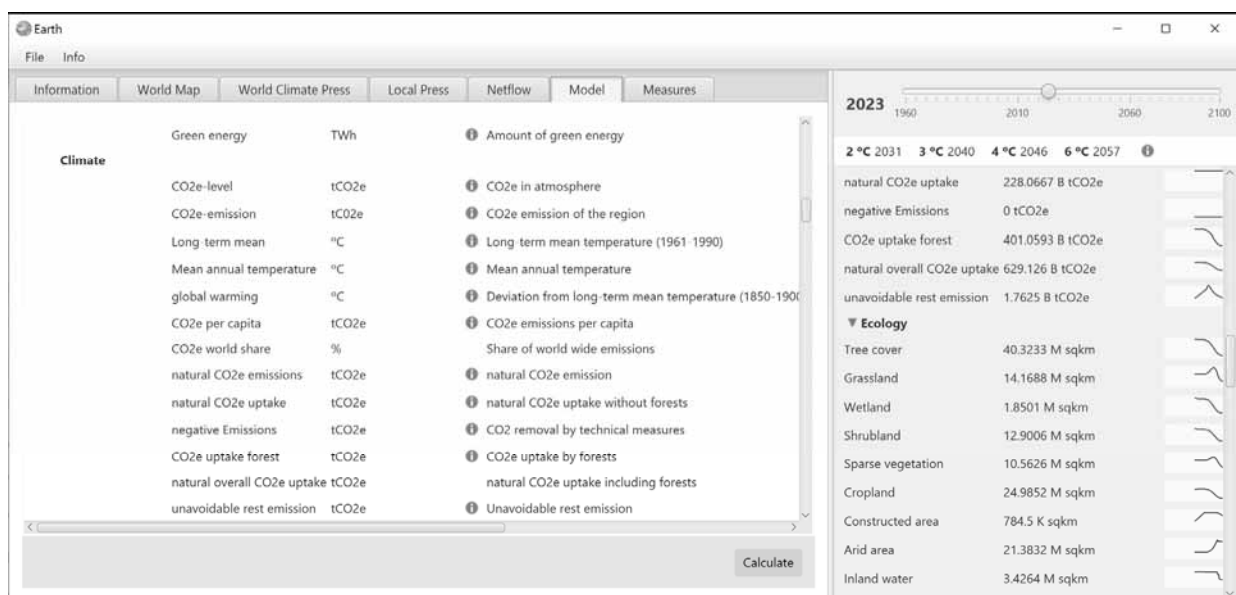

Figure 5: *MyWorld* informs the user on data used in the underlying climate model, including data sources.

The game therefore estimates the impact of climate change on natural systems and living conditions on the conservative side, turning optimistic when modelling the capacity of nature and society to mitigate the impact and to adapt to it.

The underyling simulation model employs an iterative difference equation system [28]. The system calculates the values of approx. 60 variables with an increment of one year from 1960 up to 2100. The variables come from the fields of population, climate, energy, CO2 emitters, society, ecology, and economy, and are explained to the player in detail. An individual difference equation is defined for each variable, which allows the most probable extrapolation of the value curve. Some equations use heuristics and constants taken from publications of the highest available quality, as described above. The historical variables collected from the data sources are in some cases used to adjust the parameters of the heuristics as well as possible, given the goals stated above regarding erring on the positive side.

All equations and heuristics can be controlled and partially changed in the 'Model' view (again, see Figure 5) by the user. That view also indicates for each equation whether it is based on historical data, is generated by a reliable approximation method, or consists of a plausible but basically uncertain estimation.

The predictive significance of itterated differential equations decreases with increasing t [29]. Therefore, as already described, the *MyWorld* simulation model used does not produce exact predictions of the future. Rather, it is aimed at creating plausible scenarios and developments that give the player an understanding of dependencies in the world climate system and the general impact of climate change on their future living conditions.

2.3 Mitigation Measures

As its main gaming element, *MyWorld* allows the player to define their mitigation and adaptation strategy by defining countermeasures in the 'Measures' view.

For this purpose, the player can switch on and off the default measures committed by individual countries or change their parameters, such as percentages or time targets. In additional information boxes, the player can find out how binding the commitments of the nations are, e.g., whether they are anchored in law or merely non-binding declarations of intent.

In addition to those default measures, the player can define their own measures by influencing the course of certain variables. For example, they can stipulate that a particular nation will reduce certain emissions by a fixed factor by a certain date. Depending on the adjustment of the mitigation measures, the simulation engine calculates a new course for all variables and adjusts all views accordingly. As a result, the player can develop an understanding of which measures work how well, and how ambitious the world's mitigation measures have to be to avoid negative impacts on living conditions and natural systems. That didactic effect includes also an understanding of the timeframe in which certain measures have to be implemented in order for the entire ecological and societal system to thrive in the upcoming decades.

The following model variables can be modified by user-defined measures:

Birth rate: *MyWorld* assumes that human-induced climate change is directly related to the number of people living on earth. If the user does not modify this variable, the model assumes the UN-predicted birth rates [26].

Death rate: The death rate, along with the birth rate, is also an important factor for the size of the world population. Unmodified by the user, *MyWorld* assumes that the death rate stays at the level of 2020.

State Fragility: The Fragile State Index [31] is a measure of a nation's internal security. By default, this factor assumes changes in fragility dependent on the development of the nation's gross domestic product.

Gross Domestic Product: The gross domestic product is a measure of a nation's productivity and thus of the standard of living of its citizens. By default, *MyWorld* adapts the gross domestic product dependent on the mean annual temperature of a nation.

Forestation: Forested areas are an important factor influencing the removal of CO2 from the atmosphere. If a user changes this factor by planning (de-)forestation campaigns, *MyWorld* automatically adjusts the land use of the nation. This means that the other landscape types (i.e., grassland, wetlands, shrubland, desert, sparse vegetation, and cropland) are adjusted so that the total area remains unchanged. Without specific measures present, this factor is derived from the temperature-dependent utilization model.

CO2e per capita: In *MyWorld*, this factor is the central control variable for influencing the CO2e balance of a nation. More detailed factors, such as the energy mix or the mix of emitters, cannot be influenced directly by the user, as only insufficient models exist describing how changes in more detailled factors affect a nation.

Negative Emissions: This factor indicates how much CO_2e is removed from the atmosphere by human activities. For such a carbon capture and storage strategy, various methods are potentially feasible. However, currently there are no significant capacities of negative emissions [32][33], so they are assumed to be zero by default. Since it is also currently unclear whether and when such processes could be used on a global scale, *MyWorld* does not make any pre-assumptions but leaves them to the player to schedule.

MyWorld does not prescribe in detail how targets set by mitigation measures are achieved, or why the targets might be feasible or unfeasible to reach. For many of the mentioned variables (e.g., forestation, negative emissions, and state fragility) no detailed understanding of their feasibility of implementation or impact on the course of climate change exist yet.

However, to get a better understanding of the course and impact of climate change, it is sufficient to show to a user what might happen if certain targets are reached or not reached – independent of the means of their implementation.

3 Conclusion

This paper presented *MyWorld*, a simulation-based computer game that aims at facilitating a better understanding of the progression of climate change and its impact on a user's regional living conditions, as well as the effect of potential mitigation measures on climate change and those living conditions. The paper described the game both from the user's point of view as well as the underlying simulation model.

The simulation model has been developed, implemented, and verified. A user-friendly graphical interface has been developed, giving users access to the model parameters and results. The game now is ready for extensive evaluation with stakeholders. In further research steps, the game will therefore be co-evaluated with university students from the earth sciences, municipal climate protection managers, other stakeholders, and the general public.

References

[1] Olfert, A, et al. Sustainability and resilience - a practical approach to assessing sustainability of infrastructure in the context of climate change. In: G. Hutter, M. Neubert and R. Ortlepp. *Building resilience to natural hazards in the context of climate change - Knowledge integration, implementation, and learning.* Springer, 2021.

[2] Bigio AG, Ochoa MC, Amirtahmasebi R. Climate-resilient, Climatefriendly World Heritage Cities. *Urban Development Series Knowledge Papers, Bd. 19,* World Bank, Washington, DC, 2014.

[3] Lückerath D, Milde K, Ullrich O. The ARCH project: Investigating the impact of climate change on historic areas. *Simulation Notes Europe* 2021; 31(2): 53-56.

[4] Goshua, A, et al. Addressing Climate Change and Its Effects on Human Health: A Call to Action for Medical Schools. *Academic Medicine* 2021; 96(3): 324-328.

[5] Malhi GS, Kaur M, Kaushik P. Impact of Climate Change on Agriculture and its Mitigation Strategies: A Review. *Sustainability.* 2021; 13(3): 1318.

[6] Beyer U, et al. *MyWorld – A Simulation Game about Climate Change,* http://world4us.de/en/start-english/. Accessed Feb 1, 2023.

[7] Stanitsas M, Kirytopoulos K, Vareilles E. Facilitating sustainability transition through serious gaming: a systematic literature review. *Journal of Cleaner Production.* 2019; 208: 924-936.

[8] Gerber A, Ulrich M, Wäger FX, Roca-Puigròs M, Gonçalves JSV, Wäger P. Games on Climate Change: Identifying Development Potentials through Advanced Classification and Game Characteristics Mapping. *Sustainability.* 2021; 13(4):1997.

[9] Monechi M, Ubaldi E, Gravino P, Chabay I, Loreto V. Finding successful strategies in a complex urban sustainability game. *Scientific Reports.* 2021; 11:15765.

[10] Lebel P, Sriyasak P, Kallayanamitra C, Duangsuwan C, Lebel L. Learning about climate-related risks: decisions of Northern Thailand fish farmers in a role-playing simulation game. *Regional Environmental Change.* 2016; 16, 1481-1494.

[11] Predescu A, Mocanu M. Increasing Collaboration and Participation Through Serious Gaming for Improving the Quality of Service in Urban Water Infrastructure. Abramowicz W, Corchuelo R. *Business Information Systems Workshop BIS 2019.* Lecture Notes in Business Information Processing 373. Cham: Springer, 2019.

[12] Gangolells M, Casals M, Macarulla M, Forcada N. Exploring the Potential of a Gamified Approach to Reduce Energy Use and Carbon Emissions in the Household Sector. *Sustainability*. 2021; 13: 3380.

[13] Druen PB, Zawadzki SJ. Escaping the Climate Trap: Participation in a Climate-Specific Social Dilemma Simulation Boosts Climate-Protective Motivation and Actions. *Sustainability*. 2021; 13: 9438.

[14] d'Aquino P, Bah A. Land Policies for Climate Change Adaptation in West Africa: A Multilevel Companion Modeling Approach. *Simulation & Gaming*. 2013; 44(2-3): 391-408.

[15] Kauneckis DL, Auer MR. A Simulation of International Climate Regime Formation. *Simulation & Gaming*. 2013; 44(2-3): 302-327.

[16] de Vries B. Susclime: A Simulation/Game on Population and Development in a Climate-Constrained World. *Simulation & Gaming. 1998; 29*(2): 216-237.

[17] van Pelt SC, Haasnoot M, Arts B, Ludwig F, Swart R, Biesbroek R. Communicating climate (change) uncertainties: Simulation games as boundary objects. *Environmental Science & Policy*. 2015; 45: 41-52.

[18] Lu HP, Ho HC. Exploring the Impact of Gamification on Users' Engagement for Sustainable Development: A Case Study in Brand Applications. *Sustainability*. 2020; 12: 4169.

[19] de Kraker J, Offermans A, van der Wal MM. Game-Based Social Learning for Socially Sustainable Water Management. *Sustainability*. 2021; 13: 4646.

[20] Bontchev B, Antonova A, Terzieva V, Dankov Y. Let Us Save Venice – An Educational Online Maze Game for Climate Resilience. *Sustainability*. 2022; 14: 7.

[21] Pardoux E, Talay D. Discretization and simulation of stochastic differential equations. *Acta Applicandae Mathematica*. 1985; 3: 23-47.

[22] Higham DJ. An Algorithmic Introduction to Numerical Simulation of Stochastic Differential Equations. *SIAM Review*. 2001; 43(3): 525-546.

[23] National Oceanic and Atmospheric Administration. *Global Monitoring Laboratory*. https://gml.noaa.gov/ccgg/trends/; accessed Feb 14, 2023.

[24] Intergovernmental Panel on Climate Change (IPCC). Summary for Policymakers. *Climate Change 2022: Mitigation of Climate Change. Contribution of Working Group III to the Sixth Assessment Report of the Intergovernmental Panel on Climate Change.* Cambridge University Press, Cambridge, UK and New York, NY, USA, 2022.

[25] Ritchie H, Roser M. *Our World in Data. Energy mix*. 2022. https://ourworldindata.org/energy-mix; accessed Feb 14, 2023.

[26] United Nations Department of Economic and Social Affairs, Population Division (2022). *World Population Prospects 2022: Summary of Results.* UN DESA/POP/2022/TR/NO. 3.

[27] Organisation for Economic Co-Operation and Development. *Land cover in countries and regions.* https://stats.oecd.org/Index.aspx?DataSetCode=LAND_COVER; accessed Feb 14, 2023.

[28] Mørken K. Chapter 6: Numerical Simulation of Difference Equations. *Numerical algorithms and digital representation*. Oslo, Norway: University of Oslo, 2017.

[29] Sundbye L. *Discrete Dynamical Systems, Chaos Theory and Fractals.* CreateSpace Independent Publishing Platform. 2018*, ISBN* 172716153.

[30] United Nations Department of Economic and Social Affairs, Population Division. *World Population Prospects 2022: Summary of Results.* UN DESA/POP/2022/TR/NO 3, 2022.

[31] The Fund for Peace. *Fragile State Index Annual Report 2022*. https://fragilestatesindex.org /wp-content/uploads/2022/07/22- FSI-Report-Final.pdf; accessed Feb 14, 2023.

[32] Dods MN, Kim EJ, Long JR, Weston SC. eep CCS: Moving Beyond 90% Carbon Dioxide Capture. *Environmental Science & Technology*. 2021; 55(13): 8524-8534.

[33] Yadav S, Mondal SS. A review on the progress and prospects of oxy-fuel carbon capture and sequestration (CCS) technology. *Fuel*. 2022; 308: 122057.

Analysis of Train Delays using Bayesian Networks

Valentin Barzal[1*], Matthias Rößler[2], Matthias Wastian[2],

Felix Breitenecker[1], Nikolas Popper[3]

[1]Institute of Analysis and Scientific Computing, TU Wien, Wiedner Hauptstraße 8-10,
 1040 Vienna, Austria; *valentin.barzal@tuwien.ac.at

[2]dwh GmbH, Neustiftgasse 57-59, 1070 Vienna, Austria;

[3]Institute of Information Systems Engineering, TU Wien, Favoritenstraße 11, 1040 Vienna, Austria;

Abstract. Bayesian networks can be used for analysis and representation of dependencies in large data sets. Due to their property of operating with graphs, they are suitable for analyzing delays in rail networks. After getting an overview of the theory of Bayesian networks, this article deals with recent literature about Bayesian networks and train delays. Furthermore, the presented methods will be applied to data from the Austrian railway network.

Introduction

Since public transport plays a major role in society, it is on societies behalf to keep delays to a minimum. In order to reach the goal of minimizing delays, it is important to understand not only the reasons of delays but also the propagation of delays within the public transport network. The availability of large data sets, powerful computers and suitable mathematical tools allows analyzing such delays in a sensible way.

1 Bayesian Network

A *Bayesian network* is a model represented by a directed acyclic graph (DAG) $\mathscr{G} = (V, E)$, whereat V is the vertex set and E is the edge set. Every vertex represents a random variable. There exists an edge $e \in E$ between two vertices $v, w \in V$, if and only if there is a probabilistic dependency between the two random variables represented by v and w ([1]).

Depending on the model, the random variable (i.e. vertex) can take on different types of values ([2], [3]), e.g. unordered values (e.g. *blue*, *green*, *yellow*), ordered values (e.g. *low*, *medium*, *high*) or continuous values ($\mathbb{R}$). Every random variable also has its probability distribution, which needs to be added to the graphical representation. If the random variables take on continuous values (e.g. when dealing with continuous data), we often consider *multivariate normal variables*, i.e. the random variables are normally distributed and linked by linear constraints. An example of this case is illustrated in Figure 1.
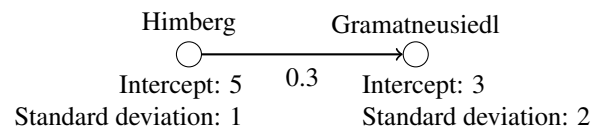

Figure 1: Considering that a train at station *Himberg* is 10 minutes late, then it is expected to be 6 minutes late ($3 + 0.3 \cdot 10 = 6$) at station *Gramatneusiedl*, with a standard deviation of 2 minutes.

When using Bayesian networks for modelling real-world problems, we often just have data describing the values of our random variables, but no information about the graph structure, i.e. the edges/dependencies between the vertices/random variables. In this case, we want to derive the graph structure from the values of the random variables. The *Max-Min Hill-Climbing* method (MMHC) enables this derivation and will be used in Section 2 and Section 3. A detailed introduction to this algorithm can be found in [4].

2 Analyzing the Long Island Rail Road System

In [1], Ulak et al. investigate network-wide pattern of rail transit delays in the Long Island Rail Road System, i.e. a railway system in New York that has a length of 620 miles and consists of a total of 11 rail lines. In Section 3, the methods used in [1] will be modified and used for data of the Austrian railway system. Therefore, Section 2 recapitulates the methods and ideas of [1] without going too deep into detail or presenting the results.

In order to build a Bayesian Network as described in Section 1, every station is considered as a random variable. It takes on the average delay at this station within a certain time interval. There should exist an edge between two vertices (i.e. between two stations) if and only if there is a dependence between those two vertices (i.e. if a delay at one station affects the occurrence of a delay at the other station).

It is possible to classify each train as either eastbound or westbound. When analyzing the delay propagation, i.e. when creating the Bayesian Network, either all eastbound or all westbound trains are considered, but not both east- and westbound trains.

By analyzing the data of an app used by the passengers, the authors receive the delay of every train at every station (with a few exceptions). The observation period is divided into 1-hour intervals. For every station the average delay per train within the examined hour is calculated. A data sample consists of the average delay time at every station within one hour. By using the *Max-Min Hill-Climbing* method (MMHC) and the maximum likelihood method, the graph structure and the corresponding parameters are compiled from the independent data samples. The R-package `bnlearn` was used for this task. Detailed documentation about this package can be found in [3].

In order to receive an expressive score for every stations role in delay propagation, two metrics are introduced. The Inducer score of station s indicates how much a delay at station s influences the delays at all the other stations. The Susceptible score of station s indicates how much the delay at station s is influenced by the delays at all the other stations. Similar scores will be introduced in Section 3 in a more precise way.

3 Analyzing the Austrian Railway System

In this section we want to modify the methods of [1] and apply them to data of the Austrian railway network. For this purpose, delay data provided by the Austrian national railway company *Österreichische Bundesbahnen (ÖBB)* is used. It not only contains information about the delay at every train station, but at every operation control point, a so-called "Betriebsstelle". These are specific points within the network. Every train station is also a operation control point. In the following, the word "station" will be used for operation control point.

3.1 Differences to the Long Island Rail Road System

The different topology of the railway network and the different timetables cause different problems that need to be faced:

- In [1], the length of every time interval is chosen to be 1 hour. Considering longer time intervals "flattens" the delays, since temporal peaks are divided by a higher number of trains. So shorter time intervals provide better "resolution" of the occurrence of delays.

  On the other hand, it takes some time to propagate the delay within the network. In Austria, there are longer distances between stops and therefore it takes longer to propagate delays. Choosing the length of the time interval to be 1 hour, most trains will "occur" in more than one time interval. Since the different data sets (i.e. delays within different time intervals) are meant to be independent, this causes some problems.

- There are stations that are not passed by any train in certain time intervals. Calculating the average delay in that period would provoke dividing by zero. This problem can be solved by considering the totaled delay instead of the average delay.

  However, this still might yield meaningful results, since the delays at a station that is approached by a lot of trains, each having just a little delay, might be more relevant than the delay at a station that is only approached by a single train, having a longer delay.

- The Long Island Rail Road System is quite crowded, i.e. if a train is delayed, it is very likely that this affects other trains. In Austria, there are

also parts where the temporal distance between different trains is much longer. In this case, delays will still propagate since a delayed train probably will still be delayed at its next stop, but it does not directly affect the delays of other trains.

- By considering only the eastbound or westbound trains, a cycle-free network was obtained in [1]. In Austria, a classification in eastbound or westbound is not possible (e.g. there are also trains going from north to south and vice versa). However, considering all the trains will lead to cycles within the network. This conflicts with the attempt of modelling the network as a directed *acyclic* graph. A strategy to resolve this problem is to delimit the number of trains considered.

- In the Long Island Rail Road System, there are just 124 stops, so it is a relatively small network. Considering all trains in Austria leads to a gigantic model (in terms of vertex numbers, edge numbers and parameters). But when examining only a selection of trains (and its corresponding stations), there are still influences from the non-considered trains. So there is "external" disturbing.

- There are also trains not operated by ÖBB using the same tracks . In the provided data there is only information about the trains operated by ÖBB. So even if no data selection is done, there will be still disturbances by other, not observed trains.

3.2 Methodology

Considering Subsection 3.1, the following restriction will be made:

- Only trains going from Vienna (station *Hauptbahnhof* or *Westbahnhof*) to St. Pölten and vice versa and the corresponding operational points between those two stations will be observed. In this case each train can be classified in eastbound or westbound and we obtain cycle-free networks. This section is also quite crowded, so there will be interactions between different trains.

- Since the distance between Vienna and St. Pölten is relatively short, we can set the length of the time intervals to 1 hour, without dealing too much with the problems mentioned in Subsection 3.1.

- We will not consider the average delay but the totaled delay of every time interval at each station.

Considering only the stations from Vienna to St. Pölten and vice versa is of course a very strong restriction but it enables us receiving suitable results. The considered stations ("Betriebsstellen") are sketched in Figure 2. In Vienna, there are two branches - one branch going to *Wien Westbahnhof* and one branch going to *Wien Hauptbahnhof*. Between the stations *Knoten Hadersdorf* and *Knoten Wagram* there are also two different routes: In the north (via *Tullnerfeld*) there is the so-called *Neue Westbahn*, in the south (via *Pressbaum*) there is the *Alte Westbahn*.

Figure 2: Considered stations (operation control points) between Vienna and St. Pölten

3.3 Network structure

Similar to [1], we use the R-package `bnlearn` (and the functions `hc` and `bn.fit`) to obtain the network structure. It was also considered to use the Python-packages `Pomegranate` and `PyMC3` for the same task, but those packages can only deal with random variables that take on unordered values . The results can be seen in Figure 3 and Figure 4. In these figures, the directions of the dependencies were not indicated.

When searching for the graph structure, we expect a graph that resembles the geographical topology of the stations, e.g. it would not make sense if a station close to St. Pölten directly affects a station close to Vienna. The topological sorting never coincides with the actual geographical order of the stations. However, we did expect such a behavior, since phenomena like backward propagation (i.e. dependencies going in the opposite direction) and others can cause a mismatch with the geographical order of the stations. Furthermore, some stations are very close and therefore have almost the same delays. In this case, the order of those stations in the obtained network is almost arbitrary.

When observing the plots visually, we detect that there are also connections between stations that are far apart. There are even connections between stations from the *Alte Westbahn* and *Neue Westbahn*, whereat these kind of connections are relatively rare.
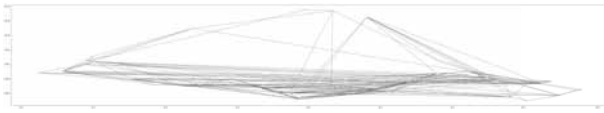
Figure 3: Network connections (eastbound). X-axis and y-axis indicate latitude and longitude.
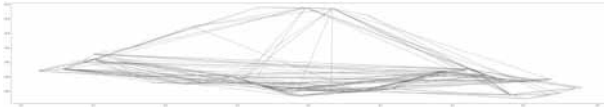

Figure 4: Network connections (westbound). X-axis and y-axis indicate latitude and longitude.

3.4 Metrics

The metrics are inspired by the metrics used in [1], but slightly modified.

The Inducer score indicates how much a delay at a station s influences the delays at all the other stations. Therefor, the delay at the examined station s is set to the median delay of this station (based on the data) and the delays at all the other stations are set to 0. Given this initial condition, the expected delay at every other station is estimated by the Bayesian network. Those values are averaged over all stations. The score of station s can be written as

$$\text{Score}_{\text{I}}(s) = \frac{1}{n-1} \sum_{\substack{i=1 \\ i \neq s}}^{n} \mathbb{E}(X_i | X_s = x_s, \mathbf{X} \backslash (X_s \cup X_i) = 0)$$

where n is the number of random variables, x_s is the median (observed) delay at station s and $\mathbf{X} = (X_i)_{i \in \{1,\dots,n\}}$ is the ensemble of all random variables.

The Susceptible score indicates how much the delay at a station s is influenced by the delays at all the other stations. Therefor, the delay at one station i (with $i \neq s$) is set to its median delay (based on the data) and the delays at all the other stations (including the examined station s) are set to 0. Given this initial condition, the expected delay at the examined station is estimated by the Bayesian network. This procedure is repeated and averaged over all stations $i \neq s$. Using the same notation as above, the score of station s can be written as

$$\text{Score}_{\text{S}}(s) = \frac{1}{n-1} \sum_{\substack{i=1 \\ i \neq s}}^{n} \mathbb{E}(X_s | X_i = x_i, \mathbf{X} \backslash (X_i \cup X_s) = 0)$$

When considering the metrics, we observe that almost all stations with the highest (top 4) scores are ei-

ther stations that are passed by all trains or stations of the *Alte Westbahn*. Only the station *Tfo* (close to Tullnerfeld) has the highest inducer score (westbound), although it is located at the *Neue Westbahn*. So the *Neue Westbahn* acts well in reducing delay propagation. Going in the westbound direction, two stations at the very beginning of the route reach high susceptible scores (*Wien Hauptbahnhof* and *Wien Westbahnhof Frachtenbahnhof*). Those stations are very susceptible to delays at other stations (although almost all stations are passed *after* those two stations). We also observe that some stations reach negative susceptible scores. According to our model, this means that delays at certain other stations reduce the delay at this observed station.

3.5 Conclusion

When applying the methods introduced in [1] to the Austrian railway system, we need to make restrictions. In order to obtain the inevitable property of an acyclic directed graph, we can only consider an area where every train can be classified into a certain (cycle-free) direction. R yields a network structure that seems partly reasonable. There are also connections between stations that are far apart and connections between *Alte Westbahn* and *Neue Westbahn*. However, this does not necessarily need to conflict with the real behaviour.

The inducer score and susceptible score indicate which stations play a big role in delay propagation. It seems reasonable that the *Neue Westbahn* acts well w.r.t. reducing delay propagation, since this section was constructed quite recently. The fact that stations at the beginning of the route have quite high susceptible scores fits to the idea of back-propagation. However, there are also stations with negative susceptible scores. This does not seem to be reasonable.

References

[1] Ulak MB, Yazici A, Zhang Y. Analyzing network-wide patterns of rail transit delays using Bayesian network learning. *Transportation Research Part C: Emerging Technologies*. 2020;119:102749.

[2] Korb KB, Nicholson AE. *Bayesian artificial intelligence*. CRC press. 2010.

[3] Scutari M, Lebre S. Bayesian networks in R: with applications in systems biology. 2013.

[4] Tsamardinos I, Brown LE, Aliferis CF. The max-min hill-climbing Bayesian network structure learning algorithm. *Machine learning*. 2006;65(1):31–78.

Solving ARGESIM Benchmark CP2 'Parallel and Distributed Simulation' with Open MPI and Matlab PCT – Lattice Boltzmann Simulation

David Jammer[1,2]*, Peter Junglas[2], Sven Pawletta[1]

[1]Research Group Computational Engineering and Automation, University of Applied Sciences Wismar,
Philipp-Müller-Straße 14, 23966 Wismar, Germany; *david.jammer@cea-wismar.de

[2]PHWT-Institut, PHWT Vechta/Diepholz, Am Campus 2, 49356 Diepholz, Germany;

Abstract. The ARGESIM benchmark CP2 consists of three different tasks to study current technologies for the parallelization of simulation programs, two of which have been addressed in a previous publication. The third one is the study of the fluid flow in a special geometry using the Lattice Boltzmann method. The task is studied with two methods for up to 256 cores, again using the MPI message passing library Open MPI and Matlab from The MathWorks in combination with the Parallel Computing Toolbox. Solutions with different grid sizes are compared with each other in terms of runtime and speedup. The Open MPI version generally shows good speedups even for large core numbers, while the Matlab version has poor results for 32 cores or more. On the other hand, the scalar Matlab version is several times faster than the Open MPI version, leading to a smaller runtime for up to 32 cores.

Introduction

In this article the solution of one task of the ARGESIM benchmark CP2 [1] will be presented. The benchmark contains three tasks, two of which have already been solved and presented in [2]. The remaining task, the Lattice Boltzmann simulation, is solved in this article. The solution is again implemented with the two technologies Open Message Passing Interface (Open MPI) [3] and Matlab Parallel Computing Toolbox (Matlab PCT)[4].

Since the description of the Lattice Boltzmann task in [1] is very sketchy, the basic method is explained in more detail in the first section, followed by a description of the scalar algorithm. Then the strategy for parallelization of this algorithm is presented. Finally, implementations in MPI and PCT are examined and compared.

The investigations were performed on an HPC system of the PHWT Institute called Seneca. The specifications of the system are shown in Table 1. All programs and scripts necessary to reproduce the results presented here are available from [5].

1 Introduction to Lattice Boltzmann Simulation

The Lattice Boltzmann Method (LBM) is a computational fluid dynamics method that has gained popularity, since it is especially well suited for parallel computers. In the following its basic ideas will be presented and the CP2 benchmark task described in full detail. This should make the task accessible to non-experts. A thorough introduction into the method and its connection to the familiar Navier-Stokes description can be found in [6].

LBM is based on the kinetic theory, which describes a fluid on a mesoscopic scale between the macroscopic description of a continuous fluid and the microscopic tracking of individual particles.

Nodes	3
Cores	288
Processors	AMD Epyc 7552
Main memory	1536 GiByte
High-speed network	100 GBit/s InfiniBand
Management network	1 GBit/s Ethernet
Operating system	OpenSuse Leap 15.3
Middleware	OpenHPC
Cluster management	Warewulf
Job Scheduler	SLURM
Software	GCC 9.3.0
	GSL 2.6
	open MPI 4.1.1
	ucx 1.13.0
	libfabric 1.13.0
	hwloc 2.1.0
	Matlab R2021a

Table 1: Seneca hardware and software overview.

Its fundamental variable is the distribution function $f(\vec{x}, \vec{\xi}, t)$, which represents the mass density of particles at position $\vec{x}$, velocity $\vec{\xi}$ and time t. It is connected to the macroscopic mass density $\rho(\vec{x}, t)$ and the macroscopic velocity $u(\vec{x}, t)$ by

$$\rho(\vec{x}, t) = \int f(\vec{x}, \vec{\xi}, t) \, d^3 \xi$$
$$\rho(\vec{x}, t) \vec{u}(\vec{x}, t) = \int \vec{\xi} f(\vec{x}, \vec{\xi}, t) \, d^3 \xi.$$

Using standard assumptions one can show that the distribution function will reach an equilibrium distribution given by

$$f^{\text{eq}}(\vec{x}, \vec{v}, t) = \rho \left(\frac{1}{2\pi R_i T} \right)^{\frac{3}{2}} e^{-v^2/(2R_i T)},$$

where the relative velocity $\vec{v} := \vec{\xi} - \vec{u}$ is the deviation of the particle velocity from the macroscopic velocity. f satisfies the Boltzmann equation

$$\frac{\partial f}{\partial t} + \xi_i \frac{\partial f}{\partial x_i} + \frac{F_i}{\rho} \frac{\partial f}{\partial \xi_i} = \Omega(f).$$

Here, $\vec{F}$ describes external forces, while Ω, the so called *collision operator*, is given by the forces between the particles during collisions. In LBM it is usually replaced by the *BGK collision operator* (named after its inventors Bhatnagar, Gross and Krook)

$$\Omega(f) = -\frac{1}{\tau}(f - f^{\text{eq}}).$$

which simply describes the evolution of f towards f^{eq}. The corresponding relaxation time τ is related to the macroscopic viscosity.

For the computation of f with LBM one discretizes space, time and velocity, choosing one of several schemes according to the dimension of the problem. Applying standard lattice units, the CP2 task uses a fixed time step $\Delta t = 1$ for t, a two-dimensional square grid with $\Delta x = \Delta y = 1$ for $\vec{x}$ and a set $\vec{c}_i$, $i = 0, \dots, 8$ of velocities $\vec{\xi}$ (cf. Fig. 1), e. g. $\vec{c}_0 = (0,0)'$, $\vec{c}_1 = (1,0)'$, $\vec{c}_5 = (1,1)'$ etc. .
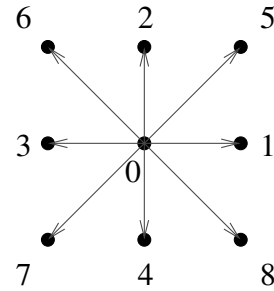
Figure 1: Velocities used in discretization scheme.

For simplicity one replaces the argument $\vec{\xi}$ with an index corresponding to one of the nine possible velocities, writing

$$f_i(\vec{x}, t) := f(\vec{x}, \vec{c}_i, t), \quad i = 0, \dots, 8$$

The macroscopic quantities are then given simply by

$$\rho(\vec{x}, t) = \sum_i f_i(\vec{x}, t)$$
$$\rho(\vec{x}, t) \vec{u}(\vec{x}, t) = \sum_i \vec{c}_i f_i(\vec{x}, t).$$

The equilibrium distribution can now be simplified to

$$f_i^{\text{eq}}(\vec{x}, t) = w_i \rho \left(1 + \frac{\vec{u}\vec{c}_i}{c_s^2} + \frac{(\vec{u}\vec{c}_i)^2}{2c_s^4} - \frac{\vec{u}\vec{u}}{2c_s^2} \right),$$

with the speed of sound $c_s = 1/\sqrt{3}$ and the weights

$$w_i = \left(\frac{4}{9}, \frac{1}{9}, \frac{1}{9}, \frac{1}{9}, \frac{1}{9}, \frac{1}{36}, \frac{1}{36}, \frac{1}{36}, \frac{1}{36}\right)'.$$

The corresponding Lattice Boltzmann Equation (LBE) in the force-free case $\vec{F} = \vec{0}$ is

$$f_i(\vec{x} + \vec{c}_i, t + 1) = f_i(\vec{x}, t) + \Omega_i(\vec{x}, t),$$

again using the BGK collision operator

$$\Omega_i(f) = -\frac{1}{\tau}(f_i - f_i^{\text{eq}}),$$

where the relaxation time is given by the viscosity ν:

$$\tau = \frac{\nu}{c_s^2} + \frac{1}{2}.$$

Finally one needs initial and boundary values and a few parameters. The CP2 task requests a quadratic lattice of size $n_x \times n_x$ with $n_x = 257$ and boundary values describing a cavity flow that has been studied in [7]: The upper grid line has a constant velocity $\vec{u}_0 = (0.1, 0)'$, while all other boundary points are fixed walls (cf. Fig. 2).
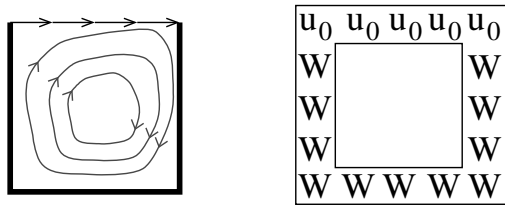
Figure 2: Definition of boundary values.

The initial values of the macroscopic properties are defined as

$$\rho(\vec{x}, 0) = 1$$
$$\vec{u}(\vec{x}, 0) = \vec{0}.$$

The end time of the simulation is given as $t_{end} = 350,000$, when a steady state should have been reached. To adapt to the much larger processing power and memory size since the publication of [1], larger grids up to $n_x = 2048$ and end time $t_{end} = 500,000$ will be studied in the following.

At last, a Reynolds number of Re = 1000 is given,

which leads to a viscosity of

$$\nu = \frac{(n_x - 1)u_{0,x}}{\text{Re}} = 0.0256.$$

2 Basic Scalar Implementation

The scalar implementation follows the lines of the basic algorithm described in [6]. The essential idea is to split the LBE in two parts, the collision step

$$f_i^*(\vec{x}, t) = f_i(\vec{x}, t) - \frac{1}{\tau}(f_i(\vec{x}, t) - f_i^{\text{eq}}(\vec{x}, t)),$$

which is a local operation at a point, and the propagation step

$$f_i(\vec{x} + \vec{c}_i, t + 1) = f_i^*(\vec{x}, t),$$

which transports the distribution to neighbouring points. Initially the distribution function is set to the equilibrium values given by $\rho(\vec{x}, 0)$ and $\vec{u}(\vec{x}, 0)$. Then the following computations are performed in a loop over time steps:

1. computation of ρ and $\vec{u}$ from f_i,

2. computation of f_i^{eq} from ρ and $\vec{u}$,

3. collision step to get f_i^*,

4. propagation step to get $f_i(\vec{x}, t + 1)$.

During the collision step the boundary behaviour is implemented: At the top line f is set to the equilibrium value defined by the given $\vec{u}_0$; at the wall points the full-way bounce-back method is used, which reverses the velocity of an incoming distribution, i.e. it sets

$$f^*(\vec{x}, \vec{c}_i, t) = f(\vec{x}, -\vec{c}_i, t).$$

After the time loop the relative magnitude $|\vec{u}|/|\vec{u}_0|$ of the macroscopic velocity is computed and plotted, as is requested in the benchmark. Fig. 3 shows the result for the standard benchmark parameters.

3 Parallel Lattice Boltzmann Simulation

In this chapter, a parallelization strategy for the Lattice Bolzmann simulation is introduced and investigated on the HPC system Seneca using two technologies.
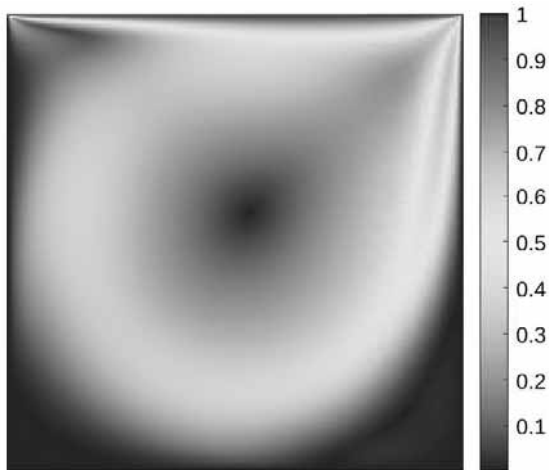
Figure 3: Relative macroscopic velocity magnitude for $n_x = 257$ after 350,000 iterations.

3.1 Parallelization Strategy

To process the Lattice Boltzmann simulation in parallel, the set of cores is virtually arranged in a two-dimensional cartesian coordinate system as shown in Figure 4. The data grid f is distributed equally along

(0,0) 0	(0,1) 1	(0,2) 2	(0,3) 3
(1,0) 4	(1,1) 5	(1,2) 6	(1,3) 7
(2,0) 8	(2,1) 9	(2,2) 10	(2,3) 11
(3,0) 12	(3,1) 13	(3,2) 14	(3,3) 15

Figure 4: Organization of cores on a two-dimensional cartesian coordinate system.

this grid, so that each core contains a section of the entire grid according to its coordinates. Except for the propagation step, all calculations on such a section can be done indepedently by each core.

To simplify the decomposition, the data grid size n_x is restricted to a power of two in the implementation, e.g. 32x32, 64x64, etc. The number of cores n_C is subject to the same condition so that the entire grid can be divided equally.

Therefore, n_C was varied from 1, 2, 4, . . . , 256 in the following measurements. Of course, an uneven distribution could be implemented easily. But a fine-grained study of the effects of the total core number would reveal more about the memory architecture and the interconnect structure of the hardware than about the properties of the high-level tools we are interested in.

In the propagation step, displacements are performed in the north, east, south and west directions, as well as the four diagonal directions. In these shifts, data must be communicated with neighboring cores. For horizontal or vertical shifts, there is at most one neighbor to send and one to receive and complete edges of the local matrix are sent or received. Data points at the global edges, which do not receive values through a shift, retain their current values. The diagonal shifts are a bit more complicated because there are more communication partners here (cf. Fig. 5). At first sight,
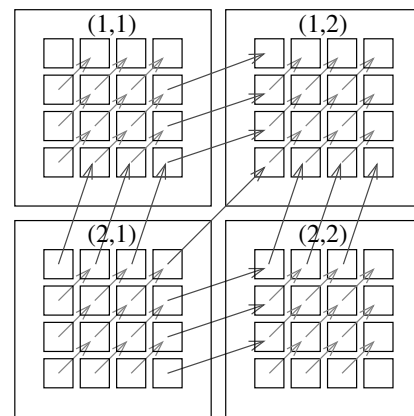
Figure 5: Matrix shift to the northeast with communication neighbors.

these operation can be simplified by combining two of the simple shift operations. For example, a shift to the north-east can be realized by shifting first to the east, then to the north. But actually, this leads to wrong values at the outer edge points, as can be seen in Fig. 6. Therefore, the following implementations are realized using explicit diagonal shifts.

A different approach is used by the ScaLAPACK library [8]: There the entire grid is divided into smaller matrices of fixed blocksize, which are then distributed cyclically across the core grid. Since this seems to lead to a much more involved communication pattern in our application, it has not been followed here.
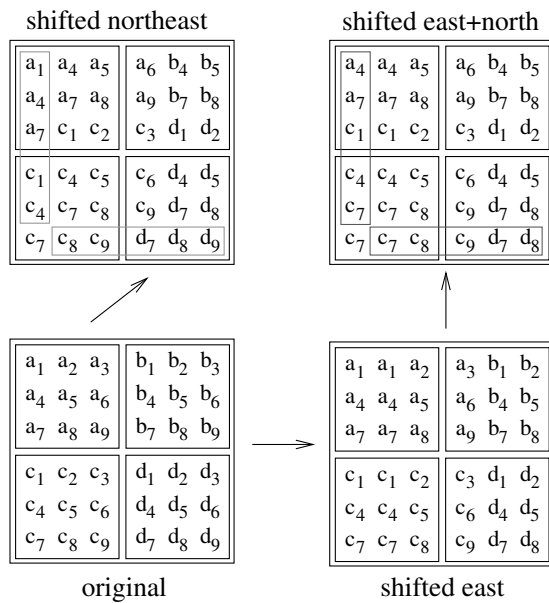
shifted northeast

a_1 a_4 a_5	a_6 b_4 b_5
a_4 a_7 a_8	a_9 b_7 b_8
a_7 c_1 c_2	c_3 d_1 d_2
c_1 c_4 c_5	c_6 d_4 d_5
c_4 c_7 c_8	c_9 d_7 d_8
c_7 c_8 c_9	d_7 d_8 d_9

shifted east+north

a_4 a_4 a_5	a_6 b_4 b_5
a_7 a_7 a_8	a_9 b_7 b_8
c_1 c_1 c_2	c_3 d_1 d_2
c_4 c_4 c_5	c_6 d_4 d_5
c_7 c_7 c_8	c_9 d_7 d_8
c_7 c_7 c_8	c_9 d_7 d_8

a_1 a_2 a_3	b_1 b_2 b_3
a_4 a_5 a_6	b_4 b_5 b_6
a_7 a_8 a_9	b_7 b_8 b_9
c_1 c_2 c_3	d_1 d_2 d_3
c_4 c_5 c_6	d_4 d_5 d_6
c_7 c_8 c_9	d_7 d_8 d_9

original

a_1 a_1 a_2	a_3 b_1 b_2
a_4 a_4 a_5	a_6 b_4 b_5
a_7 a_7 a_8	a_9 b_7 b_8
c_1 c_1 c_2	c_3 d_1 d_2
c_4 c_4 c_5	c_6 d_4 d_5
c_7 c_7 c_8	c_9 d_7 d_8

shifted east

Figure 6: Comparison of direct and composite diagonal shifts.

3.2 Open MPI

For the first parallel implementation, the C programming language and the Open Message Passing Interface (MPI) [3] were used. In order to realize the organization of the cores as a cartesian grid, Open MPI provides two functions: `MPI_Dims_create` factors the total number of cores into a balanced product. For the core numbers used here, this results either in a quadratic core grid or the size in one direction is twice the size of the other one. The function `MPI_Cart_create` then uses these sizes to create a communicator that maps the existing cores to a two-dimensional coordinate system. Due to the restrictions in grid size and total core number, the local data grid sizes of a core can then simply be calculated by dividing the total length n_x by the sizes of the core grid.

The calculation of the propagation step was divided into eight functions, one function for each direction. To identify the communication partners in north, east, south and west direction the function `MPI_Cart_shift` was used. This function returns the communication partners for sending and receiving the boundary values of the local data grids, but is restricted to shifts along the cartesian axes. It simply returns `MPI_PROC_NULL`, when a shift would leave the core grid. This value can be used safely in a send or receive function resulting in a null operation.

For the diagonal shifts, the coordinates of a core in the core grid and the corresponding target and source coordinates were determined with `MPI_Cart_coords`. They were then used to determine the corresponding ranks for the send and receive operations with `MPI_Cart_rank`. It is important to use this function only with valid coordinates, otherwise the program terminates with an error. To prevent this, one can again use the `MPI_Cart_get` function.

To collect the data at the end of the simulation the function `MPI_Cart_coords` was used to define the core with coordinates $(0,0)$ as the master and for sorting of the data. This allowed the grid segments to be associated with the correct points in the global grid.

3.3 Matlab PCT

The second parallel implementation was created using Matlab and the Parallel Computing Toolbox (PCT) [4]. A very short introduction to Matlab/PCT and the different parallelization strategies it supplies can be found in [2]. The underlying scalar version was taken from [9], which already compares different earlier parallel toolboxes from Mathworks and other authors.

For the task studied here, the PCT concept of codistributed arrays seems to be ideal: The data array is distributed to the workers automatically, and the local workers can still use the global index to address all array points. If an element is not available locally, it is sent immediately to the accessing worker. Unfortunately, the corresponding functions are badly documented and – more importantly – show an extremely bad performance [2]. Therefore, the `spmd` construct was used in the implementation, which creates a parallel section that is executed by each worker. This leads to a programming style that is smiliar to the MPI implementation. Since PCT does not provide functions for creating a two-dimensional core grid and to map cores to a grid, this functionality was implemented in the application using the functions `numlabs` and `labindex`. For convenience, an array was supplied that contains the positions of all labindex values in the core grid.

For the propagation step, separate functions were created for each of the eight directions. To determine the communication partners a function `cart2D_shift` was written, which determines the rank of the target and the source from a direction vector and a displacement. This makes it easy to determine the communication partners. The sending and receiving of the data was realized with `labSend` and `labReceive`.

After the `spmd` section the local arrays are directly available in one cell array. Therefore the merging of the results could be realized simply by rearranging all velocity data in a global array.

3.4 Comparison of solutions

The two implementations were tested on Seneca and the runtime was analyzed depending on the grid size and the number of cores. The grid size was selected from 256x256 to 2048x2048, the number of cores from 1 to 256. Since Seneca consists of three nodes with 96 cores each, runs with up to 64 cores were computed on one node using local memory only, while for 128 and 256 cores two and three nodes were utilised, and data had to be sent across the high-speed network. For small numbers of cores the number of iterations has been reduced to make the computing times feasable. The timing results have been scaled afterwards to the total number of iterations for easier comparison. The scalar overhead of the computations was negligible in these cases.

Figure 7: Runtime and speedup of the Open MPI implementation for different grid sizes.

Figure 7 shows the runtime and speedup results of the Open MPI implementation. The most basic model would assume runtimes that fall with $1/n_C$ and rise with n_x^2, which in a log-log representation would lead to parallel decreasing straight lines with constant separation. The runtime plots very roughly show this behaviour, especially for larger grid size. The deviations can be better analyzed in the speedup plot, in particular when comparing the results with the ideal case of linear speedup. Here the occuring superlinear speedup can be seen clearly, which is usually due to the memory architecture of the system: With increasing core number, the local memory decreases, until it fits in a fast cache memory. This interpretation is supported by the observation that the point, where superlinear speedup begins, rises with grid size and core number in such a way that the local memory size stays constant. Another expected behaviour is the drop of speedup for large core numbers, when more than one node is used. This effect gets smaller with rising grid size, because the amount of computation dominates the rising communication times. The results suggest that for large grid sizes an even higher speedup can be reached with more cores. In Figure 8 the results of the Matlab implementation are presented.

Looking at the speedups, Matlab PCT reaches good to reasonable values for up to 16 cores, but very poor results for more cores. The drop in performance at 128 cores can be seen again, except for a very peculiar rise at the grid size $n_x = 2048$. But when comparing the runtimes, the image changes completely: The table 2, which displays the runtimes for the scalar case $n_C = 1$, shows the impressive performance of Matlab compared to the direct C implementation. This is probably due to the efficient matrix operations Matlab is based on.
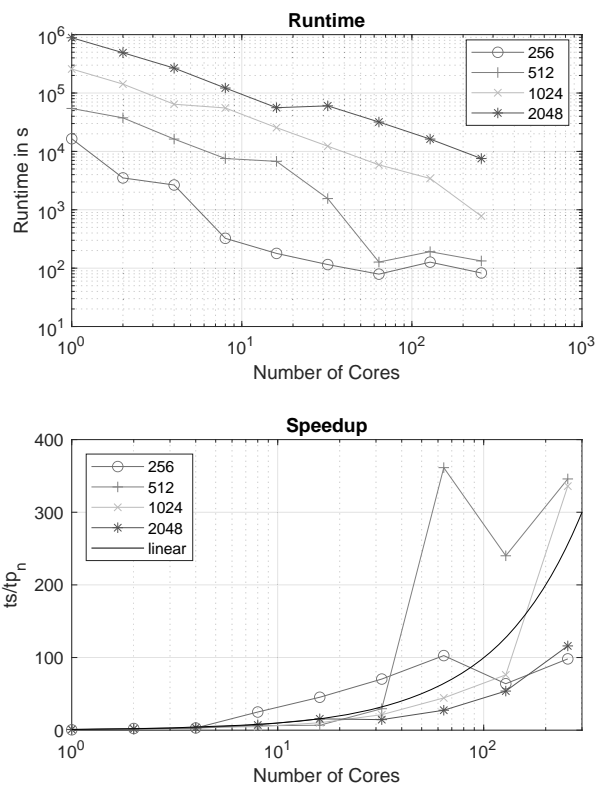
grid size	runtime [min] Open MPI	runtime [min] Matlab PCT	ratio
256	274.4	36.1	7.59
512	906.3	175.6	5.16
1024	4297.3	1173.1	3.66
2048	14757.2	4347.6	3.39

Table 2: Comparison of runtimes for $n_C = 1$.
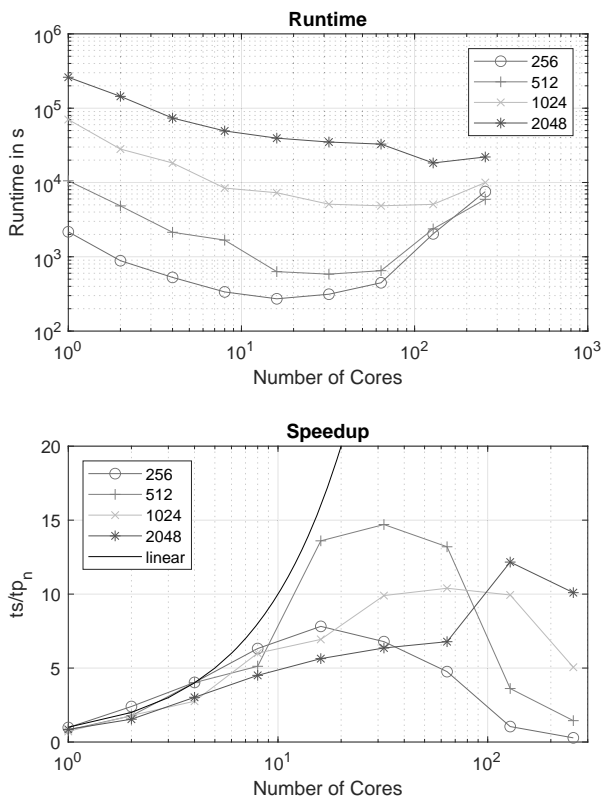
Figure 8: Runtime and speedup of the Matlab PCT implementation for different grid sizes.

Figure 9: Ratio of Runtimes for MPI and Matlab implementations.

Figure 9 shows the runtime ratios of the parallel Open MPI and Matlab PCT versions, compared for the same number of cores. Apart from the case of small grid size, Matlab is faster for up to 32 cores, and for the larger grids even up to 64 cores. It takes a lot of cores, until the better speedup of Open MPI catches up with the better scalar performance of Matlab PCT.

4 Conclusion

The goal of the CP2 benchmark cannot be to compare latest parallelization strategies for current hardware architectures – this would require much more complex algorithms such as those studied in the HPCG benchmark [10]. Instead, the underlying question of the benchmark is: How can non-experts use tools and computing environments to take advantage of modern multi-core CPUs? Correspondingly, the MPI implementations of the three CP2 tasks that have been presented here and in [2] mainly serve as points of reference and use well known techniques, whereas the parallelization methods

and outcomes provided by a scientific computing environment such as Matlab are the main point of interest.

In this respect Matlab PCT is a very interesting approach, but the results presented here show that it doesn't quite live up to its prospects. On the one hand the `spmd` construct and standard message-passing methods make it possible to reach reasonable speedups for small core numbers, but require knowledge of standard parallelization techniques. Furthermore, the `parfor` command provides a convenient tool for very simple cases like Monte Carlo studies. On the other hand, the promising concept of codistributed arrays provides a very elegant way to cope with the distribution and parallel processing of large matrices, but it has shown very poor performance even in the simple PDE task.

For very compute-intense applications, which benefit most from larger core numbers, one typically would resort to standard languages like C or C++, together with optimizing compilers. But as we have seen in the PDE and LBM tasks, Matlab can be compatible or even better in the scalar case, due to its highly optimized mathematical libraries. Therefore it would be very desirable, if Matlab PCT could sustain good speedups to larger numbers of cores.

In spite of its interesting topic, the ARGESIM CP2 benchmark has not been addressed before. To some extent, this might be due to the rather short description of the Lattice Boltzmann task, which needs background reading to understand the algorithm at all. Hopefully, the short introduction provided here can help as a starting point for further studies.

Another problem of CP2 is the small problem size. To make the tasks challenging on modern architectures, one has to scale up the problem sizes considerably. Maybe, one could modernize this benchmark by using scaling methods instead of fixed sizes, and reissue it as a new entry in the standard ARGESIM benchmark suite, giving up on the idea of a special "parallel benchmarks" series.

References

[1] Breitenecker F, Höfinger G, Pawletta T, Pawletta S, Hinz R. ARGESIM Benchmark on Parallel and Distributed Simulation. *SNE Simulation News Europe*. 2007;17(1):53–56. ISSN 0929-2268.

[2] Jammer D, Junglas P, Pawletta S. Solving ARGESIM Benchmark CP2 'Parallel and Distributed Simulation' with Open MPI/GSL and Matlab PCT - Monte Carlo and PDE Case Studies. *SNE Simulation Notes Europe*. 2022;32(4):211–220. DOI: 10.11128/sne.32.bncp2.10625.

[3] Graham RL, Woodall TS, Squyres JM. Open MPI: A flexible high performance MPI. *Lecture notes in computer science*. 2006;3911:228.

[4] The MathWorks. *MATLAB Parallel Computing Toolbox*.
URL `https://de.mathworks.com/help/` `pdf_doc/parallel-computing/` `parallel-computing.pdf`

[5] CEA Wismar. *ARGESIM benchmark CP2 on GitHub*. `https:` `//github.com/cea-wismar/ArgesimCP2`.

[6] Krüger T, Kusumaatmaja H, Kuzmin A, Shardt O, Silva G, Viggen EM. *The Lattice Boltzmann Method: Principles and Practice*. Cham, Switzerland: Springer. 2017.

[7] Hou S, Zou Q, Chen S, Doolen GD, Cogley AC. Simulation of cavity flow by the lattice Boltzmann method. *Journal of computational physics*. 1995; 118(2):329–347.

[8] Blackford LS, Choi J, Cleary A, D'Azevedo E, Demmel J, Dhillon I, Dongarra J, Hammarling S, Henry G, Petitet A, Stanley K, Walker D, Whaley RC. *ScaLAPACK Users' Guide*. Philadelphia, PA: Society for Industrial and Applied Mathematics. 1997.

[9] Fink R. Untersuchungen zur Parallelverarbeitung mit wissenschaftlich-technischen Berechnungsumgebungen. Ph.D. thesis, Universität Rostock, Rostock. 2007.

[10] Dongarra J, Heroux MA, Luszczek P. A new metric for ranking high-performance computing systems. *The International Journal of High Performance Computing Applications*. 2016;30(1):3–10.

EUROSIM Data and Quick Info

EUROSIM CONGRESS 2023
July 3-5, 2023, Amsterdam, The Netherlands www.eurosim2023.eu

ASIM SPL 2023 20th ASIM Dedicated Conference on
Simulation in Production and Logistics
September 13-15, 2023, Ilmenau, Germany www.asim-fachtagung-spl.de

I3M 2023 International Multidisciplinary Modeling & Simulation Multiconference
September 18-20, 2023, Athens, Greece
www.msc-les.org/i3m2023

SIMS 2023 – 64. Int. Conference
September 26-27, 2023, Västerås
www.scansims.org

Winter Simulation Conference 2023,
December 10-13, 2023,
San Antonio, TX, USA **www.wintersim.org**

EUROSIM – the **Federation of European Simulation Societies** was set up in 1989.

The purpose of EUROSIM is to provide a European forum for simulation societies and groups to promote modelling and simulation in industry, research, and development – by publication and conferences.

www.eurosim.info

EUROSIM members may be national simulation societies and regional or international societies and groups dealing with modelling and simulation.

Full Members are ASIM, CEA-SMSG, CSSS, DBSS, KA-SIM, LIOPHANT, LSS, PTSK, NSSM, SIMS, SLOSIM, UKSIM. Observer Members are ALBSIM and ROMSIM. Former Members (societies in re-organisation) are: CROS-SIM, FRANCOSIM, HSS, ISCS.

EUROSIM is governed by a B**oard** consisting of one representative of each member society, president, past president, and SNE representative.

President	M. Mujica Mota (DBSS), *m.mujica.mota@hva.nl*
Past President	Emilio Jiménez (CEA-SMSG), *emilio.jimenez@unirioja.es*
Secretary	*P. M. Scala (DBSS), paolo.scala@fedex.com*
Treasurer	Felix Breitenecker (ASIM) *felix.breitenecker@tuwien.ac.at*
Webmaster	Irmgard Husinsky (ASIM), *irmgard.husinsky@tuwien.ac.at*

SNE **– Simulation Notes Europe** is EUROSIM's membership journal with peer reviewed scientific contributions about all areas of modelling and simulation, including new trends as big data, cyber-physical systems, etc.

The EUROSIM societies distribute e-SNE in full version to their members as official membership journal. The basic version of e-SNE is available with open access. Publishers are EUROSIM, ARGESIM and ASIM,

www.sne-journal.org
office@sne-journal.org

SNE-Editor: Felix Breitenecker (ASIM)
felix.breitenecker@eic@sne-journal.org

EUROSIM Congress and Conferences

Each year a major EUROSIM event take place, as the EUROSIM CONGRESS organised by a member society, SIMS EUROSIM Conference, and MATHMOD Vienna Conference (ASIM).

EUROSIM Congress 2023, the *11th EUROSIM Congress*, will be organised by DBSS, the Dutch Benelux simulation society, in Amsterdam, July 3-5, 2023:

www.eurosim2023.eu

Furthermore, EUROSIM Societies organize local conferences, and EUROSIM co-operates with the organizers of I3M Conference and WinterSim Conference Series:

www.msc-les.org/i3m2023
www.wintersim.org/

EUROSIM Member Societies

ASIM
German Simulation Society
Arbeitsgemeinschaft Simulation

ASIM is the association for simulation in the German speaking area, servicing mainly Germany, Switzerland and Austria.

President	Felix Breitenecker, *felix.breitenecker@tuwien.ac.at*
Vice President	Sigrid Wenzel, *s.wenzel@uni-kassel.de* Thorsten Pawletta, *thorsten.pawletta@hs-wismar.de* Andreas Körner, *andreas.koerner@tuwien.ac.at*

ASIM is organising / co-organising the following international conferences: **ASIM SPL** Int. Conference 'Simulation in Production and Logistics' (biannual), **ASIM SST** 'Symposium Simulation Technique' (biannual), **MATH-MOD** Int. Vienna Conference on Mathematical Modelling (triennial). Furthermore, **ASIM** is co-sponsor of *WSC* - Winter Simulation Conference and of the *I3M* and conference series.

ASIM Working Committees

GMMS: Methods in Modelling and Simulation
    U. Durak, umut.durak@dlr.de
SUG: Simulation in Environmental Systems
    J. Wittmann, wittmann@informatik.uni-hamburg.de
STS: Simulation of Technical Systems
    W. Commerell, commerell@hs-ulm.de
SPL: Simulation in Production and Logistics
    S. Wenzel, s.wenzel@uni-kassel.de
EDU: Simulation and Education
    A. Körner, andreas.koerner@tuwien.ac.at
Working Group Big Data: Data-driven Simulation in
    Life Sciences, N. Popper, niki.popper@dwh.at
Other Working Groups: Simulation in Business Administration, in Traffic Systems, for Standardisation, etc.

Contact Information

www.asim-gi.org

info@asim-gi.org, admin@asim-gi.org

ASIM – Inst. of Analysis and Scientific Computing, TU Wien, Wiedner Hauptstraße 8-10, 1040 Vienna, Austria

CEA-SMSG – Spanish Modelling and Simulation Group

CEA is the Spanish Society on Automation and Control. The association is divided into national thematic groups, one of which is centered on Modeling, Simulation and Optimization (**CEA-SMSG**).

President	José L. Pitarch, *jlpitarch@isa.upv.es*
Vice President	Juan Ignacio Latorre, *juanignacio.latorre@unavarra.es*

Contact Information

www.ceautomatica.es/grupos/

simulacion@cea-ifac.es

CEA-SMSG / Emilio Jiménez, Department of Electrical Engineering, University of La Rioja, San José de Calasanz 31, 26004 Logroño (La Rioja), Spain

CSSS – Czech and Slovak Simulation Society

CSSS is the Simulation Society with members from the two countries: Czech Republic and Slovakia. The CSSS history goes back to 1964.

President	Michal Štepanovský *michal.stepanovsky@fit.cvut.cz*
Vice President	Mikuláš Alexík, *alexik@frtk.fri.utc.sk*

Contact Information

cssim.cz

michal.stepanovsky@fit.cvut.cz

CSSS – Český a Slovenský spolek pro simulaci systémů, Novotného lávka 200/5, 11000 Praha 1, Česká republika

DBSS – Dutch Benelux Simulation Society

The *Dutch Benelux Simulation Society* (DBSS) was founded in July 1986 in order to create an organisation of simulation professionals within the Dutch language area.

President	M. Mujica Mota, *m.mujica.mota@hva.nl*
Vice President	A. Heemink, *a.w.heemink@its.tudelft.nl*
Secretary	P. M. Scala, *paolo.scala@fedex.com*

Contact Information

www.DutchBSS.org

a.w.heemink@its.tudelft.nl

DBSS / A. W. Heemink, Delft University of Technology, ITS – twi, Mekelweg 4, 2628 CD Delft, The Netherlands

KA-SIM Kosovo Simulation Society

The Kosova Association for Modeling and Simulation (KA-SIM) is closely connected to the University for Business and Technology (UBT) in Kosovo.

President	Edmond Hajrizi, *ehajrizi@ubt-uni.net*
Vice President	Muzafer Shala, *info@ka-sim.com*

Contact Information

www.ubt-uni.net

ehajrizi@ubt-uni.net

Dr. Edmond Hajrizi
Univ. for Business and Technology (UBT)
Lagjja Kalabria p.n., 10000 Prishtina, Kosovo

LIOPHANT Simulation

LIOPHANT Simulation is a non-profit association born in order to be a trait-d'union among simulation developers and users; LIOPHANT is devoted to promote and diffuse the simulation techniques and methodologies; the Association promotes exchange of students, sabbatical years, organization of International Conferences, courses and internships focused on M&S applications.

President	A.G. Bruzzone, *agostino@itim.unige.it*
Director	E. Bocca, *enrico.bocca@liophant.org*

Contact Information

www.liophant.org

info@liophant.org

LIOPHANT Simulation, c/o Agostino G. Bruzzone, DIME, University of Genoa, Savona Campus, via Molinero 1, 17100 Savona (SV), Italy

LSS – Latvian Simulation Society

The Latvian Simulation Society (LSS) has been founded in 1990 as the first professional simulation organisation in the field of Modelling and simulation in the post-Soviet area.

President	Yuri Merkuryev, *merkur@itl.rtu.lv*
Vice President	Egils Ginters, *egils.ginters@rtu.lv*

Contact Information

www.itl.rtu.lv/imb/

merkur@itl.rtu.lv, Egils.Ginters@rtu.lv

Prof. Yuri Merkuryev, Dept. of Modelling and Simulation, Riga Technical University, Kalku street 1, Riga, LV-1658, Latvia

NSSM – National Society for Simulation Modelling (Russia)

NSSM – The National Society for Simulation Modelling (Национальное Общество Имитационного Моделирования – НОИМ) was officially registered in Russia in 2011.

President	R. M. Yusupov, *yusupov@iias.spb.su*
Chairman	A. Plotnikov, *plotnikov@sstc.spb.ru*

Contact Information

www.simulation.su

yusupov@iias.spb.su

NSSM / R. M. Yusupov, St. Petersburg Institute of Informatics and Automation RAS, 199178, St. Petersburg, 14th line, h. 39

PTSK – Polish Society for Computer Simulation

PTSK is a scientific, non-profit association of members from universities, research institutes and industry in Poland with common interests in variety of methods of computer simulations and its applications.

President	Tadeusz Nowicki, *Tadeusz.Nowicki@wat.edu.pl*
Vice President	Leon Bobrowski, *leon@ibib.waw.pl*

Contact Information

www.ptsk.pl

leon@ibib.waw.pl

PSCS, 00-908 Warszawa 49, ul. Gen. Witolda Urbanowicza 2, pok. 222

SIMS – Scandinavian Simulation Society

SIMS is the Scandinavian Simulation Society with members from the five Nordic countries Denmark, Finland, Norway, Sweden and Iceland. The SIMS history goes back to 1959.

President	Tiina Komulainen, *tiina.komulainen@oslomet.no*
Vice President	Erik Dahlquist, *erik.dahlquist@mdh.se*

Contact Information

www.scansims.org

vadime@wolfram.com

Vadim Engelson, Wolfram MathCore AB, Teknikringen 1E, 58330, Linköping, Sweden

SLOSIM – Slovenian Society for Simulation and Modelling

The Slovenian Society for Simulation and Modelling was established in 1994. It promotes modelling and simulation approaches to problem solving in industrial and in academic environments by establishing communication and cooperation among corresponding teams.

President	Goran Andonovski, *goran.andonovski@fe.uni-lj.si*
Vice President	Božidar Šarler, *bozidar.sarler@fs.uni-lj.si*

Contact Information

www.slosim.si

slosim@fe.uni-lj.si, vito.logar@fe.uni-lj.si

SLOSIM, Fakulteta za elektrotehniko, Tržaška 25, SI-1000, Ljubljana, Slovenija

UKSIM - United Kingdom Simulation Society

The UK Modelling & Simulation Society (UKSim) is the national UK society for all aspects of modelling and simulation, including continuous, discrete event, software and hardware.

President	David Al-Dabass, *david.al-dabass@ntu.ac.uk*
Secretary	T. Bashford, *tim.bashford@uwtsd.ac.uk*

Contact Information

uksim.info

david.al-dabass@ntu.ac.uk

´ UKSIM / Prof. David Al-Dabass, Computing & Informatics, Nottingham Trent University, Clifton lane, Nottingham, NG11 8NS, United Kingdom

Observer Members

ROMSIM – Romanian Modelling and Simulation Society

ROMSIM has been founded in 1990 as a non-profit society, devoted to theoretical and applied aspects of modelling and simulation of systems.

Contact Information

florin_h2004@yahoo.com
ROMSIM / Florin Hartescu, National Institute for Research in Informatics, Averescu Av. 8 – 10, 011455 Bucharest, Romania

ALBSIM – Albanian Simulation Society

The Albanian Simulation Society has been initiated at the Department of Statistics and Applied Informatics, Faculty of Economy at the University of Tirana, by Prof. Dr. Kozeta Sevrani.

Contact Information

kozeta.sevrani@unitir.edu.al

Albanian Simulation Goup, attn. Kozeta Sevrani, University of Tirana, Faculty of Economy , rr. Elbasanit, Tirana 355, Albania

Former Societies / Societies in Re-organisation

- CROSSIM – *Croatian Society for Simulation Modelling*
  Contact: Tarzan Legović, *Tarzan.Legovic@irb.hr*
- FrancoSim – Société Francophone de Simulation
- HSS – Hungarian Simulation Society
  Contact: A. Gábor, *andrasi.gabor@uni-bge.hu*
- ISCS – Italian Society for Computer Simulation

The following societies have been formally terminated:

- MIMOS –Italian Modeling & Simulation Association; terminated end of 2020.

Association Simulation News

ARGESIM is a non-profit association generally aiming for dissemination of information on system simulation – from research via development to applications of system simulation. ARGESIM is closely co-operating with EUROSIM, the Federation of European Simulation Societies, and with ASIM, the German Simulation Society.
ARGESIM is an 'outsourced' activity from the *Mathematical Modelling and Simulation Group* of TU Wien, there is also close co-operation with TU Wien (organisationally and personally).

→ **www.argesim.org**

→ *office@argesim.org*

→ ARGESIM/Math. Modelling & Simulation Group,
  Inst. of Analysis and Scientific Computing, TU Wien
  Wiedner Hauptstrasse 8-10, 1040 Vienna, Austria
  Attn. Prof. Dr. Felix Breitenecker

ARGESIM is following its aims and scope by the following activities and projects:
- Publication of the scientific journal SNE – *Simulation Notes Europe* (membership journal of EUROSIM, the *Federation of European Simulation Societies*) – *www.sne-journal.org*
- Organisation and Publication of the ARGESIM Benchmarks for *Modelling Approaches and Simulation Implementations*
- Publication of the series ARGESIM Reports for monographs in system simulation, and proceedings of simulation conferences and workshops
- Publication of the special series FBS Simulation – Advances in Simulation / Fortschrittsberichte Simulation - monographs in co-operation with ASIM, the German Simulation Society
- Support of the Conference Series MATHMOD Vienna (triennial, in co-operation with EUROSIM, ASIM, and TU Wien) – www.mathmod.at
- Administration of ASIM (German Simulation Society) and administrative support for EUROSIM *www.eurosim.info*
- Simulation activities for TU Wien

ARGESIM is a registered non-profit association and a registered publisher: ARGESIM Publisher Vienna, root ISBN 978-3-901608-xx-y and 978-3-903347-xx-y, root DOI 10.11128/z…zz.zz. Publication is open for ASIM and for EUROSIM Member Societies.

SNE – Simulation Notes Europe

The scientific journal SNE – Simulation Notes Europe provides an international, high-quality forum for presentation of new ideas and approaches in simulation – from modelling to experiment analysis, from implementation to verification, from validation to identification, from numerics to visualisation – in context of the simulation process. SNE puts special emphasis on the overall view in simulation, and on comparative investigations. Furthermore, SNE welcomes contributions on education in/for/with simulation.

SNE is also the forum for the ARGESIM Benchmarks on *Modelling Approaches and Simulation Implementations* publishing benchmarks definitions, solutions, reports and studies – including model sources via web.

SNE Editorial Office /ARGESIM

→www.sne-journal.org
  office@sne-journal.org, eic@sne-journal.org

  Johannes Tanzler (Layout, Organisation)
  Irmgard Husinsky (Web, Electronic Publishing)
  Felix Breitenecker EiC (Organisation, Authors)
  ARGESIM/Math. Modelling & Simulation Group,
  Inst. of Analysis and Scientific Computing, TU Wien
  Wiedner Hauptstrasse 8-10, 1040 Vienna, Austria

SNE, primarily an electronic journal, follows an open access strategy, with free download in a basic version (B/W, low resolution graphics). SNE is the official membership journal of EUROSIM, the *Federation of European Simulation Societies*. Members of (most) EUROSIM Societies are entitled to download the full version of e-SNE (colour, high-resolution graphics), and to access additional sources of benchmark publications, model sources, etc. (group login for the 'publication-active' societies; please contact your society). Furthermore, SNE offers EUROSIM Societies a publication forum for post-conference publication of the society's international conferences, and the possibility to compile thematic or event-based SNE Special Issues.

Simulationists are invited to submit contributions of any type – *Technical Note*, *Short Note*, *Project Note*, *Educational Note*, *Benchmark Note*, etc. via SNE's website:

→ **www.sne-journal.org,**

ASIM Books – ASIM Book Series – ASIM Buchreihen

Simulation for a Sustainable Future

July, 3-5, 2023, Amsterdam, The Netherlands

The 11th edition of the EUROSIM Congress is dedicated to a sustainable future. And there is no better place than Amsterdam for celebrating the link between simulation and sustainability.

Topics and Tracks:

- Passenger Operations – Chairs: Michael Schultz, Bundeswehr University Munich
- Simulation/Optimization– Chairs: Idalia Flores, National University of Mexico- Mario L Rus, University of Córdoba Spain
- Simulation in Agroindustries– Chairs: Rodrigo Romero Silva, Wageningen University
- Simulation and Data – Chairs: Arnold Heemink, TU Delft
- Simulation for Digital Twins in Industry and Logistics – Chair:Francesco Longo/ Antonio Padovano, University of Calabria
- Methodology and Risk Assessment – Prof. Edmond Hajrizi, UBT
- Supply Chain Management, Logistics and Transportation – Chair M. Bagamanova, AUAS – Peter Meincke, DLR
- Industrial Case Studies
- Complex, Intelligent, Adaptive and Autonomous Systems (CIAAS)
- Environment and Sustainability Applications – Chairs: L. M. Fernández-Ahumada & M. Varo -Martinez, U. of Córdoba
- Simulation and ML Technology– Chair Dr. Mohammad Dehghani, Northeastern University
- Rare Events Analysis
- Gaming
- Epidemiological
- PhD & MSc/Bach Award – Chairs Dr. Luis Manuel Fernández-Ahumada, U. of Córdoba – Dr Miguel Mujica Mota, Amsterdam U. of Applied Sciences
- Multimodal Transport Simulation – Chairs: Raquel Salamanca, ISDEFE; Ashish Verma, IISC, Bangalore
- Simulation in Human Behaviour – Chairs: Jose Maria Ortiz-Gomez, Zayed University/ Christina Rott, Vrije Universiteit Amsterdam
- Simulation in Education– Cristina Ruiz Martin, Carleton University
- Agent-based Simulation – Hai Xiang Lin, TU Delft
- Energy Transition
- Aviation Track – Chairs: Benedikt Badanik, U. of Zilina -Miguel Mujica Mota, AUAS- Bruno Desart EUROCONTROL
- Monitoring and Control – Chairs: Dr. Igor Škrjanc, University of Ljubljana
- Healthcare Applications – Chair: Nikki Popper, TU WIEN
- Hybrid Simulation
- Manufacturing Applications – Chairs Dr. Antonella Petrillo&Dr. Fabio de Felice, U.of Napoli "Parthenope"
- Circular Economy – Chairs: Abdel Al Makhloufi & Amir Ghasemi, Amsterdam U. of Applied Sciences
- Military Applications – Chair Oliver Rose, Bundeswehr University
- Advanced Tutorials/workshops
- Applications in Engineering and Architecture –
- Financial Simulation
- Extraction Industries
- Poster Session – Chair Dr. Paolo Scala, Fedex

www.eurosim2023.eu

As the largest European simulation conference for production and logistics, every two years the ASIM Dedicated Conference presents forward-looking trends and current developments, scientific papers and interesting applications in the industry.

The thematic focus of the next conference is sustainability in production and logistics. Thus, the conference will address an important social issue and at the same time focus on current research topics in the simulation world.

Keynotes:

Sustainable transformation of industrial production - illustrated by the example of climate-friendly steel production
Prof. Dr. Thomas S. Spengler, Lehrstuhl für Produktion und Logistik; TU Braunschweig

Digital Twins – A Journey from Particle Physics at CERN to Industry 4.0 Manufacturing in Singapore
Dr. Peter Lendermann, D-SIMLAB Technologies Ptd Ltd, Singapore

Reports from research and teaching, development and industrial use are deliberately placed on an equal footing. Workshops and tutorials, an evening dialog event as well as the accompanying company exhibition with software vendors and service providers of the simulation industry create, in addition to the scientific program, manifold opportunities for in-depth discussions and for getting to know current topics and offers. Presentations are available in German and English.

We look forward to welcoming you to Ilmenau in September 2023.

Registration for the conference is now open. Secure your early bird discount with your registration until 07/01/2023.

www.asim-fachtagung-spl.de/asim2023/en/